UNIVERSITY OF OKLAHOMA
GRADUATE COLLEGE

ACTIVATION OF MURINE DENDRITIC CELLS THROUGH STING PATHWAY INTERACTIONS WITH GLYCATED CHITOSAN

A THESIS

SUBMITTED TO THE GRADUATE FACULTY

in partial fulfillment of the requirements for the

Degree of

MASTER OF SCIENCE

By

GHAINAA ABOUSLEIMAN

Norman, Oklahoma

2024

ACTIVATION OF MURINE DENDRITIC CELLS THROUGH
STING PATHWAY INTERACTIONS WITH GLYCATED CHITOSAN

A THESIS APPROVED FOR THE
STEPHENSON SCHOOL OF BIOMEDICAL ENGINEERING

BY THE COMMITTEE CONSISTING OF

Dr. Wei R. Chen, Chair

Dr. John Clegg

Dr. Qinggong Tang

Acknowledgment

I extend my deepest gratitude to my Principal Investigator and Chair of my thesis committee, Dr. Wei R. Chen. Without his invaluable guidance, unwavering support, and mentorship I would not have been able to embark on this journey. His encouragement of individual academic pursuits allowed me to explore several interesting facets of the research in the lab, expanding both my knowledge base and skill set. Dr. Chen also provided me with the opportunity to attend the 2024 Annual Cancer Research Symposium, where I was able to present my work to peers and fellow professionals within the cancer research community. I am profoundly thankful for Dr. Chen's guidance, which has been instrumental in shaping my academic journey and contributing to the completion of this thesis.

This journey would not have been possible without the committee members, Dr. John Clegg, and Dr. Qinggong Tang, for their efforts in advising me during the past two years and for their time to read, edit, and comment on my thesis.

I would also like to extend my gratitude to Dr. Ashley Hoover who has been a great source of inspiration for this project as well instrumental in guiding me throughout this thesis work. Dr. Hoover not only shared her wealth of knowledge with me but taught me many skills, helping me to be the researcher I am today. Her instruction helped to continue my drive froward with this research despite many hurdles along the way. I wish her well on her endeavors outside academia and hope for the opportunity to work with one another again.

I am also deeply grateful to Dr. Tingting Gu whose expertise in image analysis was of great help on this thesis work. I want to thank her for the time and patience she granted me and hope the opportunity to work together again arises.

I would also like to express my thanks to Dr. Kaili Liu and Ms. Yuanhong Sun. I want to sincerely thank them for their dedication of time, efforts, and knowledge.

Sincere thanks to Dr. William Berry who gave me many beneficial insights into the field of genomics through his collaboration on this thesis.

Thanks should also go to Vinit Sheth whose vast knowledge and expertise in microscopy made many of these possible. His patience and willingness to help allowed me to make great progress and taught me so much about imaging analysis and techniques.

I cannot leave the University of Oklahoma without thanking my fellow lab members: Trisha Valerio, Coline Furrer, Brian Baharestani, Sayre Tillery, Emeline Masquelin, Malayna Unkel, and Jacob Adams. Their continued support and help throughout my academic journey made this project possible.

Lastly, I am thankful to my parents, my brother, and my sister. Their emotional support and belief in me kept my motivation and my spirits high.

Table of Contents

List of Tables

List of Figures

Abstract

N-dihydrogalactochitosan (Glycated Chitosan, GC) is a promising immunoadjuvant for cancer therapeutics. Synthesized from chitin and galactose, GC stimulates the innate and adaptive antitumor immune responses more potently than its parent molecule, chitosan, giving it great potential for therapeutic applications. However, the cellular mechanisms of GC have yet to be fully investigated. In previous studies, it has been demonstrated that GC has strong interactions with dendritic cells (DCs) where interactions of stimulator of interferon genes (STING) and the stimulation of type I IFN are essential for the antitumor response. The activation of DCs via the STING pathway has been shown to lead to inflammatory cell death that further enhances the antitumor response and recruitment of antigen presenting cells. Herein we investigated STING-GC interactions within murine DCs, using immunofluorescence (IF), western blotting, and bulk RNA sequencing analysis to determine STING-GC colocalization in the lysosome. Using the Western blot, lysates isolating the cellular components of murine dendritic cells allowed for identification of STINGs location following GC stimulation. Within the lysosomal isolate, increased expression of STING was observed, indicating STING trafficking to the lysosome post GC stimulation. IF antibody staining allowed visualization of cellular vesicles, STING, and GC. By tagging lysosomal markers (LAMP 1) and STING, it can be seen that STING and GC are contained within swollen intracellular vesicles indicating cell stress. Through bulk RNA sequencing analysis of wild type and STING knockout (KO) mice, an upregulation of lysosomal genes dependent on STING were detected indicating immunogenic cell death (ICD) via lysosomal activity is occurring. Furthermore, upregulation of genes associated with the NLRP3 pathway was visualized post GC stimulation indicating cross talk between GC, STING, and NLRP3 pathway ICD. Visualizing the GC-STING relation is an important step in identifying the cellular mechanisms of GC, paving the way for further understanding of GC's immunological mechanism and the optimization of therapeutic applications using GC as an immunostimulant.

Keywords: N-dihydrogalactochitosan (Glycated Chitosan, GC), immunostimulant/adjuvant, immunogenic cell death, dendritic cells, STING, NLRP3, cellular mechanisms.

Chapter 1 Introduction

1.1. Immunoadjuvants and Immunostimulants

Immunostimulants encompass a diverse groups of chemicals that enhance the immune systems or drive specific immune responses through cellular interactions [1]. Their use can first traced back to 1891 when William B. Coley injected patients biological toxins as a form of cancer therapy [2]. His treatment was successful in shrinking malignant tumors and this become one of the first examples of immunotherapy. There are various types of immunostimulants ranging from natural compounds to synthetic drugs and vaccines. Their overall goal is to strengthen the body's immune response. Their primary mechanism involves the activation of key immune cells, notably macrophages and dendritic cells, thus orchestrating a cascade of immunological events that resulted in an overall heightened immune response. This is beneficials for health conditions where the immune responses is essential such as infections and cancer malignancies.

Immunoadjuvants are a subcategory within immunostimulants that stand as vital elements within vaccine formulations. Immunoadjuvants are substances that serve to enhance the immune response in conjugation with specific vaccine antigens [3]. They represent essential components within immunotherapy and vaccine development, serving to augment the body's immune response toward specific antigens. Their use can be traced as far back as the 1920s when veterinarian Gaston Ramon demonstrated that the addition of specific substances to diphtheria toxoid vaccine lead to an increased formation on antibodies in response to the vaccine and local inflammation indicating increased immune activity [4], [5]. Distinguished by their diverse compositions, including aluminum salts (such as alum), oil-in-water emulsions, liposomes, and certain bacterial derivatives, these agents play a fundamental role in fortifying the efficacy of vaccines [6], [7]. Their mechanism is similar to immunostimulants in that APCs are recruited culminating in an amplified and sustained immune reaction. This enhanced response allows for increased vaccine efficiency by necessitating smaller antigen quantities, a critical advantage in vaccine production and distribution, particularly in resource-constrained settings or during disease outbreaks. Their utilization represents a crucial facet of both vaccine design and therapeutic strategies aimed at empowering the body's defenses against various diseases.

Immunostimulants and immunoadjuvants have emerged as promising cancer therapies. Their desirability compared to other treatment modalities is rooted in their ability to amplify the body's natural defenses against various diseases, including cancer. The use of these agents has been instrumental in enhancing the effectiveness of vaccines and immunotherapies, reducing the required antigen doses, and thereby mitigating potential side effects. Furthermore, advancements in biotechnology and molecular biology have facilitated the development of highly specific and targeted agents, optimizing their efficacy while minimizing adverse reactions [8]. As research continues to unfold, the intricate dynamics between these agents and the immune system are expected to offer novel insights, potentially paving the way for innovative therapeutic strategies that are both effective and safe.

1.2. Immunostimulants in Cancer Therapy

Cancer is a condition characterized by the uncontrolled proliferation of abnormal cells, with various forms that can manifest throughout the body. Its diverse forms—ranging from solid tumors to hematologic malignancies—can manifest throughout the body [9]. When cancer metastasizes or spreads, it frequently becomes life-threatening. Metastasis accounts for over 90% of cancer-related deaths [10]. In response to this challenge, a range of cancer treatments has been developed, including surgery, chemotherapy, and radiation therapy. However, many of these conventional therapies neglect to aid the patient's immune system in its antitumor defense, thereby limiting its efficacy. This is where immunotherapies have shown promise in changing the field of cancer therapeutics.

Surgery is commonly employed when a tumor is a compact mass that can be excised with sufficient margins [11]. Nonetheless, complete removal is not always feasible due to factors such as tumor location, size, or metastasis. In such cases, chemotherapy and radiation therapy come into play. Chemotherapy involves administering powerful drugs to target and destroy rapidly dividing cancer cells throughout the body [12]. Unfortunately, this approach lacks specificity, affecting healthy cells alongside malignant ones. Consequently, patients often experience systemic side effects such as nausea, hair loss, and compromised immune function. Moreover, chemotherapy's efficacy varies, and complete control of tumors remains attainable. Radiation therapy, on the other hand, employs high-energy radiation beams to kill cancer cells or slow their growth [13]. While it can be precisely targeted, it may also affect nearby healthy tissues. Like chemotherapy, radiation therapy faces limitations in fully regulating the complex tumor microenvironment, where immune responses and other factors play pivotal roles. While chemotherapy and radiation therapy target cancer cells, these treatments overlook the intricate tumor microenvironment. This is where the value of immunotherapy becomes evident. Immunotherapy harnesses the body's own immune system to combat malignant cells, properly regulating the tumor microenvironment and holding the promise of targeted and durable outcomes.

Research indicates that cancer cells can manipulate the immune system, evading its detection and destruction. This immune evasion is a key factor contributing to the development and progression of cancer [14]. As a result, there exists a need to stimulate the immune system to aid in its recognition and elimination of tumor cells; from this need immunotherapy was born. The concept behind immunotherapy is elegant: rather than directly attacking the tumor, it empowers the immune system to do the heavy lifting. Checkpoint inhibitors, cancer vaccines, and adoptive T-cell therapies are among the diverse immunotherapeutic approaches that have shown remarkable potential [15]. These strategies aim to activate or augment specific components of the immune system, such as T-cells, natural killer cells, and dendritic cells, which play pivotal roles in immune surveillance and response [16].Central to this endeavor are immunostimulants—bioactive compounds that enhance the immune response to antigens, thereby magnifying the efficacy of vaccines and therapeutic interventions. Among these, N-dihydrogalactochitosan (Glycated Chitosan, GC) has emerged as a remarkable candidate, displaying distinctive properties that stimulate the immune system in several beneficial ways.

1.3. Glycated Chitosan as an Immunostimulant

Glycated Chitosan (GC) is a mucoadhesive immunostimulatory polymer of β-0-4-linked N-acetylglucosamine that is solubilized by the conjugation of galactose glycans [17]. It has been shown to primarily interact with phagocytic cells, such as dendritic cells and macrophages [18], [17].

GC is synthesized from chitosan and galactose with enhanced immune stimulating properties. Chitosan is a natural polysaccharide derived from Chitin which is primarily found in the shells of crabs, crayfish, and other crustaceans. It has a wide range of therapeutical use due to its biocompatibility, non-toxicity, and biodegradability [19]. However, Chitosan is largely insoluble in water, greatly limiting its biological applications [20]. In contrast, GC is water soluble and retains the biological properties of its parent molecule chitosan increasing it suitability for *in-vivo* applications [20].

1.4. Dendritic Cell Antitumor Response

Dendritic cells (DCs) are professional antigen presenting cells (APCs) that serve as a bridge between the innate and adaptive arms of the immune system [21]. DCs are known as initiators of immune responses; they are phagocytes that capture and present antigens to T-cells.

DCs serve as watchers of the immune system, strategically positioned in tissues where they continuously sample their microenvironment for foreign or aberrant antigens. Upon capturing these antigens via phagocytosis DCs undergo a process of maturation, characterized by enhanced expression of co-stimulatory molecules and increased cytokine production [22]. This maturation process primes DCs to effectively interact with T cells, fostering the development of an adaptive immune response. In the context of tumor immunity, dendritic cells play a crucial role in recognizing and responding to cancer-specific antigens [23]. Several studies have highlighted the importance of DCs in capturing antigens derived from tumors, processing them into immunogenic peptides, and presenting these peptides to T cells. This antigen presentation is a pivotal step in the activation of cytotoxic T lymphocytes (CTLs), which are instrumental in the elimination of cancer cells [24].

The crosstalk between DCs and other immune cells, such as natural killer cells and B cells, further amplifies the anti-tumor immune response. DCs contribute to the formation of tertiary lymphoid structures within tumors, creating an immunologically active microenvironment that fosters sustained anti-tumor immunity [23]. Additionally, DCs participate in the establishment of immunological memory, ensuring a rapid and potent response upon re-exposure to tumor antigens. In the tumor microenvironment, DCs play an active role of uptaking tumor DNA [25]. When the DC cell senses the DNA is foreign, Simulation of interferon genes (STING) is activated. This pathway has emerged as a central facilitator of inflammation at sites of tissue damage, infection, and cellular stress; as such it plays a key role in the immune systems antitumor response [26].

1.5. The Objectives of this Study

GC is a novel immunostimulant that primarily interacts with APCs such as dendritic cells. However, the exact mechanism of these interactions remains undiscovered. Our previous

studies have shown that GC interacts with the STING mechanism within murine DCs resulting in type I IFN and IL-1β release [27]. The objective of this study is to investigate if these interactions are the result of direct binding with GC and how this mechanism leads to immunogenic cell death (ICD).

This master's thesis is organized into four main sections. First, the overall STING pathway will be highlighted where our previous work demonstrates that there is a connection between the STING pathway and uptake of GC by DCs. In the following section, the initial steps of this pathway are demonstrated where western blotting is utilized to illustrate how stimulation with GC leads to increased STING trafficking to the lysosome. This trafficking is known to lead to cellular swelling and death illustrated in the next section through immunofluorescence tracking GC, STING, and lysosomal activity throughout the cell. The final section aims to elucidate the bigger picture, using bulk RNA sequencing to highlight trends of upregulation in genes associated with lysosomal death and the NLRP3 pathway following GC stimulation.

Chapter 2 STING Pathway

2.1. Overview

The STING pathway is a crucial component of the innate immune system that plays a vital role in the detection of cytosolic DNA and the initiation of an immune response [28], [29]. In the context of dendritic cells, STING activation can enhance the efficacy of immunotherapy by promoting the activation of dendritic cells and the priming of T cells [30]. A recent study has shown that type 1 conventional dendritic cells (cDC1s) are essential for STING-mediated rejection of multiple established and metastatic murine tumors [31]. This response is crucial in DCs' antitumor response leading to ICD and the production of pro-inflammatory cytokines. This pathway is activated when cyclic GMP-AMP synthase (cGAS) recognizes cytosolic DNA and produces cyclic GMP-AMP (cGAMP), which then binds to STING [29]. This binding leads to the activation of downstream signaling pathways, including the production of type I interferons (IFNs) and other cytokines, which help to activate both innate and adaptive immune responses [32].

Within the context of their anti-tumor activities, DCs activate STING pathway in response to the detection of cytosolic DNA, a common feature in cancer cells [33]. The process begins with DNA sensors, such as cGAS, recognizing and binding to cytosolic DNA [34]. Subsequently, cGAS catalyzes the synthesis of cyclic GMP-AMP (cGAMP), which acts as a second messenger that binds to the STING protein on the endoplasmic reticulum membrane of DCs. This binding induces a conformational change in STING, leading to the activation of the STING pathway. Following this change, the STING pathway can have several mechanisms, two of which, production of IFN-β and STING signaling leading to lysosomal cell death, will be highlighted. The first leads to the release of pro-inflammatory cytokines and the second results in immunogenic cell death.

2.2. STING Pathway Leading to Proinflammatory Cytokine Release by DCs

The activation of STING leading to the downstream release of proinflammatory cytokines is one of the most well-known pathways involving cGAS-STING signaling. The activation of STING in DCs is mediated by the TBK1-IRF3 interaction [28]. Activated STING is incorporated into protein complex II (COPII) vesicles where it traffics to the ER-Golgi intermediate compartment (ERGIC) [35]. It then recruits and activates TBK1, which phosphorylates the transcription factor IRF3. This phosphorylation event prompts IRF3 to translocate to the nucleus and initiate the transcription of genes encoding type I interferons, such as interferon-β (IFN-β). The production of type I interferons and other pro-inflammatory cytokines by DCs, driven by the STING pathway, enhances their antigen-presentation capacity. This activation, in turn, facilitates the cross-presentation of tumor antigens to CD8+ cytotoxic T cells, contributing to the generation of a robust and effective adaptive immune response against the tumor. Harnessing the STING pathway within DCs represents a promising avenue in cancer immunotherapy, offering potential strategies to bolster the anti-tumor immune response and improve therapeutic outcomes. **Figure 1** illustrates an overview of the cGAS-STING pathway leading to the production of IFN-β.

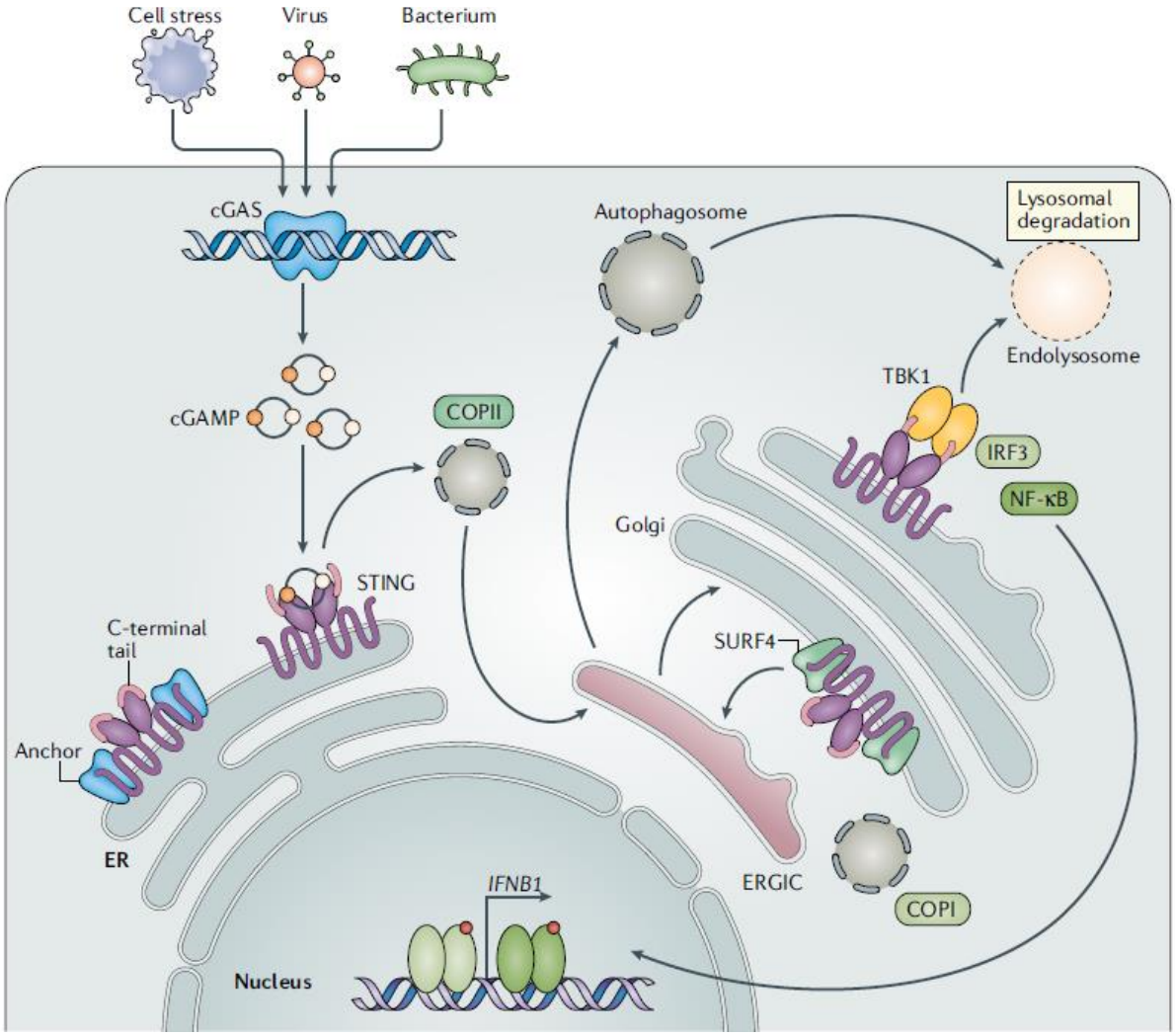

Figure 1: Overview of the cGAS-STING pathway. Detection and binding of double-stranded DNA results in a conformational change of cGAS to 2'3' cyclic GMP–AMP (cGAMP). cGAMP then binds to stimulator of interferon genes (STING) residentially located in the endoplasmic reticulum. STING then trafficking to the ER–Golgi intermediate compartment (ERGIC) via coatomer protein complex II (COPII). Here STING recruits TANK-binding kinase 1 (TBK1) leading to TBK1 autophosphorylation and STING phosphorylation along with the recruitment of interferon regulatory factor 3 (IRF3). This then enables IRF3 dimerization and translocation to the nucleus to induce the gene expression of type I interferons and other proinflammatory cytokines. Post IRF3 interaction STING traffics to the lysosome for degradation. Reproduced from Decout et. al with permission from Springer Nature [26].

Upon activation, STING undergoes dynamic subcellular trafficking, moving from the endoplasmic reticulum (ER) to the Golgi apparatus and subsequently to the lysosomes [36]. STING is transported from the ER to the Golgi apparatus by COPII-coated vesicles [37]. These vesicles are responsible for the transport of proteins and lipids from the ER to the Golgi apparatus. Once STING reaches the Golgi apparatus, it is transported to the lysosome by a process called autophagy. Autophagy, a cellular mechanism responsible for the degradation and recycling of cellular components, emerges as a key player influenced by STING activity [38]. The interplay between STING and autophagy suggests that STING may contribute to the maintenance of cellular homeostasis by regulating autophagic responses, potentially impacting the clearance of damaged organelles and proteins.

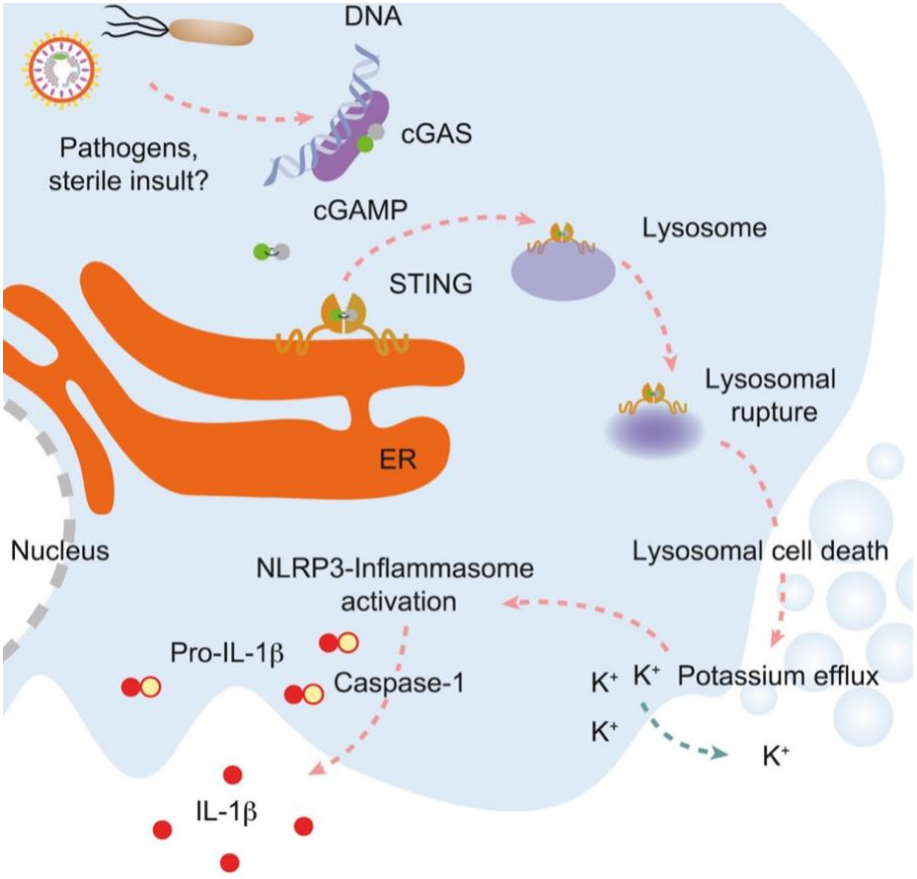

Figure 2: Cross talk between the cGAS-STING pathway and NLRP3 mediated cell death. The cGAS-STING-NLRP3 begins similarly to the beforementioned STIMG pathway with the detection of foreign DNA leading to STING activation via cGAMP. This then leads to STING trafficking to the lysosome resulting in lysosomal membrane permeabilization (LMP). LMP then leads to lysosome cell death and subsequently potassium efflux into the cell. Potassium efflux then activates the NLRP3 pathway [41] leading to activation of Caspase-1. This then leads to the release of proinflammatory cytokines such as IL-1β. Reproduced from Gaidt et. al with permission from Elsevier [40].

2.3. STING Activation Leading to Lysosomal Leakage and Cell Death

While STING aids with cell-cell communication through cytokine release, it can also lead to ICD. Depending on the cellular context and the stage of the immune response, STING exhibits a dynamic localization pattern. Recently there have been studies demonstrating crosstalk between the STING and NLRP3 pathways, with evidence suggesting that STING activation can promote NLRP3 inflammasome activation and subsequent pyroptotic cell death [39]. It is proposed that STING-mediated type I interferon production may sensitize cells to NLRP3 inflammasome activation, although the precise molecular mechanisms underlying this crosstalk remain an area of active research. The NLRP3 inflammasome is a multi-protein complex consisting of NLRP3, the adaptor protein ASC (apoptosis-associated speck-like protein containing a caspase recruitment domain), and pro-caspase-1. NLRP3 can be activated by a variety of stimuli, including pathogens, toxins, and cellular stressors, leading to its oligomerization and assembly of the inflammasome complex. Once assembled, the NLRP3 inflammasome recruits pro-caspase-1 via ASC, leading to its autocatalytic cleavage and

activation into active caspase-1. Activated caspase-1 cleaves gasdermin D (GSDMD), releasing its N-terminal fragment. The N-terminal fragment of GSDMD forms pores in the plasma membrane, leading to a rapid influx of water and ions, causing cell swelling and lysis. This form of programmed cell death is known as pyroptosis, and it is characterized by the release of proinflammatory cytokines and damage-associated molecular patterns (DAMPs), which further propagate inflammation and immune responses. An outline of the relative mechanism and its upstream activation by STING can be seen in **Figure 2** as a STING response to a pathogen. In this study, Gaidt et al. shows STING activation resulting in lysosomal cell death and interactions with the NLRP3 pathways [40]. In this mechanism STING traffics to the lysosome after binding with cGAMP. This results in lysosome membrane permeabilization and lysosomal cell death. From this, there is an influx of potassium ions which is a known activator of the NLRP3 pathway [41]. The lysosomal cell death caused by STING activation leads to the release of DAMPs and tumor-associated antigens (TAAs) into the extracellular space. These molecules are recognized by the immune system as danger signals, which leads to the activation of the immune system and the elimination of cancer cells.

2.4. GC STING Interactions

When DCs and macrophages undergo GC stimulation, there is an increase of proinflammatory cytokines. This has been previously confirmed through enzyme-linked immunosorbent assay (ELISA). In our previous studies, Hoover et. al, this was hypothesized to be a result of STING pathway activation [27]. In order to further investigate this, Bulk RNA sequencing was conducted on both wild-type and STING knockout (KO) bone marrow derived dendritic cells (BMDCs). The STING KO BMDCs were derived from mice that had been genetically modified to no longer express the STING protein. With endogenous STING removed, patterns in gene expression could be evaluated for STING dependance. Genes associated with the STING pathway were then collected and cross referenced with the data from the bulk RNA sequencing procedures. The heat maps from this analysis can be seen in **Figure 3.**

Figure 3a shows there is an upregulation of genes associated with the STING pathway when mice were administered GC [27]. This indicates that the STING pathway is actively involved in the cell's response to GC. STING dependency can be seen as much of upregulation is specific to wild type mice– there is upregulation within this experimental group when compared to the STING KO group. In **Figure 3b** the experimental groups with the largest distance between them is the wild type unstimulated and wild type GC stimulated. This indicates that GC stimulation results in large transcriptional profile changes within STING associated genes. With both of these trends observed, it is hypothesized that the cellular mechanism of this ICD is mediated through the STING pathway. When APCs are stimulated with GC they undergo ICD which in turn further stimulates the immune system recruiting more cells to the site of cell death. This leads into the purpose of this project which is to confirm STING and GC interactions to further elucidate the ICD pathway occurring within DCs post GC stimulation.

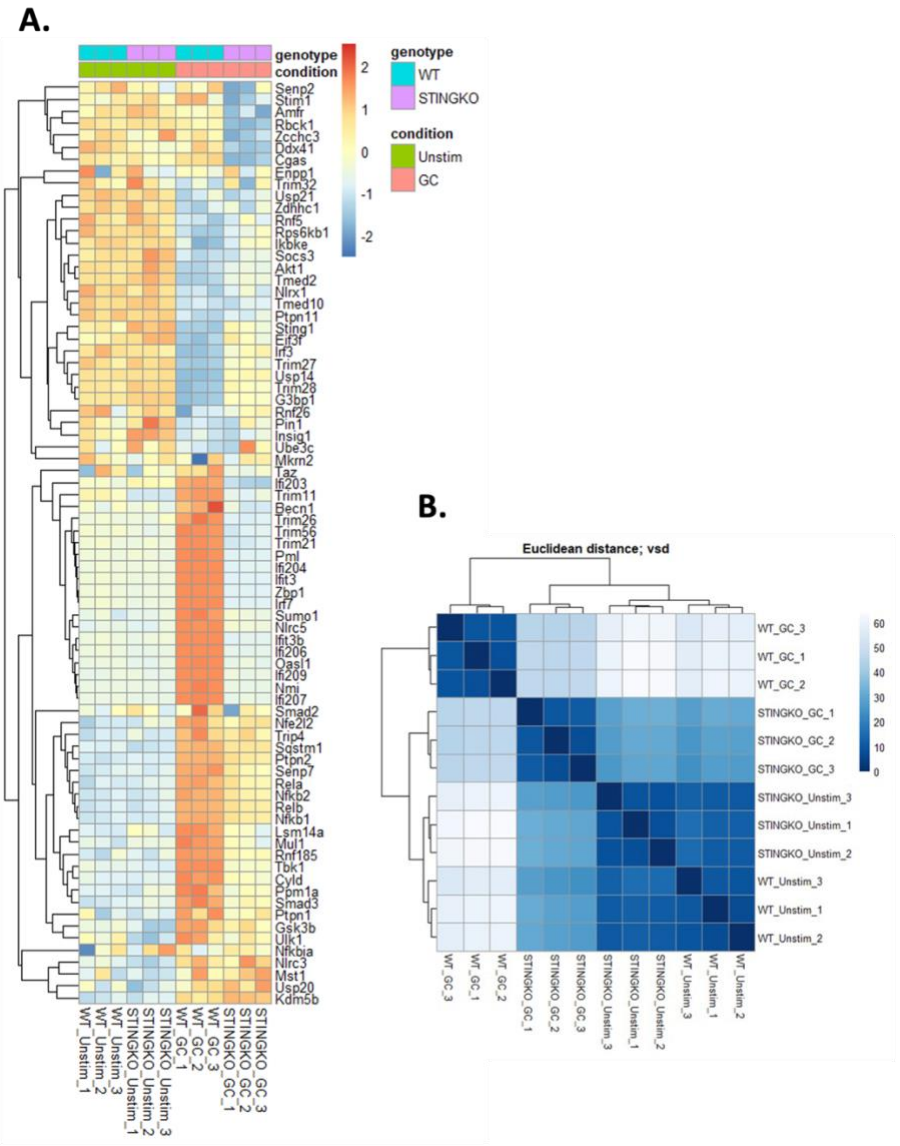

Figure 3: Heat maps illustrating STING pathway activation in the presence of GC. Panel A shows genes associated with the STING pathway and their expression levels within their experimental group. It can be seen that there is a correlation between effected STING pathway genes and GC stimulation. Panel B shows sample to sample distances through variance stabilizing transformation (vsd). The greatest distance is between WT_unstim and WT_GC indicating GC causes large transcriptional profile changes. WT_unstim represents the untreated wild type mice, STINGKO_unstim are STING knockout mice in the untreated control group, WT_GC are wild type mice that received GC vaccination, and STINGKO_GC are STING knockout mice that received GC vaccination. Figure adapted from Hoover et. al [27].

2.5. Hypothesis and Graphical Abstract

Because the STING pathway is critical for GC-induced anti-tumor and anti-viral immune responses, it is important to determine the mechanism of GC through its activation of STING pathway. The hypothesized GC-STING interaction is depicted in **Figure 4**. The first step is to confirm GC-STING interactions and colocalization in the lysosome. Then, it the long-term purpose of this study to verify the hypothesized GC-STING interactions through NLRP3 pathway,

cell death, and IFNβ release, as indicated in **Figure 4**. This is critical in determining the overall cause of cell death: if cell death is a result of K^+ efflux initiating the NLRP3 pathway or if GC leakage itself causes lysosomal membrane permeabilization (LMP).

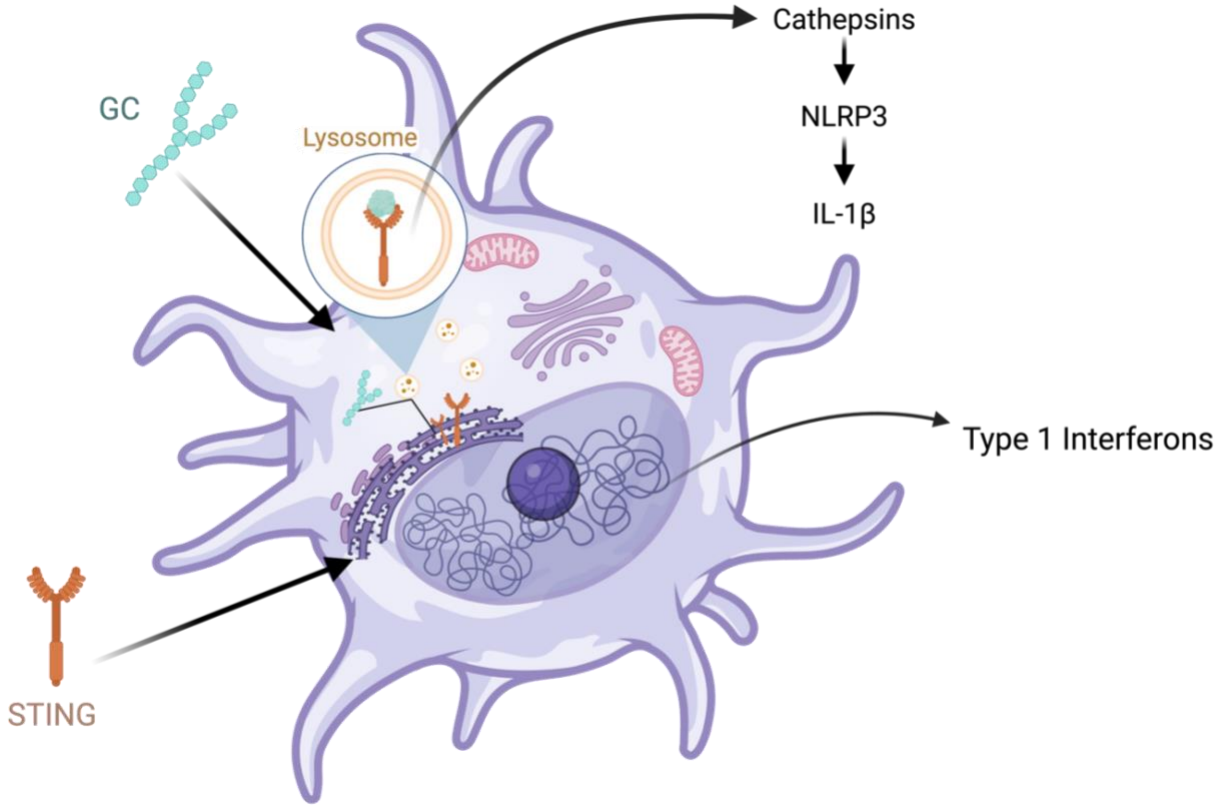

Figure 4: **Overview of hypothesized STING-GC interactions**. Here GC enters the DC cell via phagocytosis. After entering the cell, GC directly binds to STING initiating STING trafficking through the cell. Post binding, STING traffics to the lysosome which in turn initiates LMP. This results in lysosomal content leakage and K+ efflux activating the NLRP3 pathway. This pathway results in ICD and the release of proinflammatory cytokines such as IL-1β. Activation of the STING pathway also results in the release of proinflammatory cytokines such as type I IFN.

Our previous work guided the decision for both time point and GC concentration seen throughout the study. Throughout the study, the 10hr time point will be investigated and a stimulation concentration of 8μg/mL utilized. In our beforementioned study linking GC uptake to the STING pathway, several time points were investigated. Flow cytometry was conducted over a 0-24 hour time course was evaluated as well as RNA sequencing collected at the 24 hour time point. Within this study, it was found that BMDC death occurred between 10 and 16 hours with IL-1β production occurring subsequently at the 16 hour time point [27]. From this, a time point of 10 hours was chosen to observe GC-STING interactions directly prior to cell death.

At low doses GC was found to not induce cell death, but rather initiates STING-mediated release of type 1 interferons. This was supported in the previous study, where IFNβ was produced at the 6 to 10 hour time points upon stimulation with 0.8μg/mL of GC [27]. At this concentration there was no production of IL-1β and no cell death indicating the production of IL-1β and IFNβ are independent of one another. IL-1β began at a concentration of 4μg/mL and at 8μg/mL IL-1β production increased further and IFNβ production decreased [27]. Cell death

began at the 4μg/mL and increased 8μg/mL leading to 8μg/mL GC stimulation being chosen for this study. This would allow the findings to primarily focus on the cell death induced by GC.

The following thesis study utilizes the 10-hour time point and a GC concentration of 8μg/mL, however, previously a live cell study was initiated. This study was unsuccessful due to limitations in the cell model. The study utilized the DC 2.4 cell line which was found to no longer be an accurate model for the *in-vivo* conditions. An overview of this study can be found in the supplementary materials, **Appendix A and B**. Due to these findings, this study utilizes BMDCs to most closely mimic the native environment.

Chapter 3: Glycated Chitosan Induces Increased STING Trafficking to the Lysosome

3.1. Purpose

The purpose of this experimentation is to investigate the effect of GC on STING trafficking to the lysosome. This will be done through western blotting where the lysates tested will be different subcellular components of BMDCs.

3.2. Materials

Aqueous solution of N-dihydrogalactochitosan, also referred to as glycated chitosan (GC), (10mg/mL) was provided by ImmunoPhotonics, Inc. Male and female 8-12 weeks old C57BL/6J mice were purchased from Jackson Laboratories. Sex was varied to eliminate sex-associated immune differences and the age range 8-12 weeks was utilized as it an ideal age range for BMDC generation [42], [43].

3.3. Methods

3.3.1. Preparation of Bone Marrow Derived Dendritic Cells

The murine mesenchymal stem cells were extracted from the hind legs of C57BL/6J mice through dissection of the hip bone, femur, and tibia and flushing the bone marrow out of the bone using a syringe and PBS. The red blood cells were then lysed using ACK lysis buffer (Thermo Fisher, Cat# A1049201) and the cells plated at a seeding density of 10E6 cells per plate on 150mm well plates. Granulocyte-macrophage colony-stimulating factor (GM-CSF), a cytokine known to regulate DC homeostasis, was used to differentiate the stem cells to dendritic cells [44]. An initial concentration of 20ng/mL GM-CSF it utilized on day 0 to promote DC development in vitro (BioLegend, Cat# 576306). On day 3, 10mL of fresh RPMI + 20ng/mL GM-CSF med ia was added. On day 6 the media was fully changed and on day 7 the cells were extracted. Prior to stimulation, primary DC cells are present in the semi-adhere and non-adherent cell population; extraction of cells was facilitate by pipetting up and down, recovering the media, and centrifuging to pellet cells [45]. The cells were when resuspended in RPMI + 5ng/mL GM-CSF and ready for use.

3.3.2. Preparation of Lysates for Western Blot

Western blot lysates were prepared using two different methods. The first method utilized was subcellular fractionation which yielded five lysates, three of which were used. Lysosomal isolation was used to derive the final lysate.

Prior to fractionation, the BMDCs were harvested via pipetting up and down and collecting the semi adherent and suspended cells. The cells were then reseeded in 150mm well plates at a concentration of 1 million cells/ mL and stimulated with 8ug/mL of GC. The cells were then allowed to stimulate for 10 hours before using EDTA (RPI, Cat# E14000-250.0) to collect the adherent cells to be used in the following protocols.

The cellular fraction was performed using the Subcellular Protein Fractionation Kit for Cultured Cells (Thermo Fisher, Cat#78840). The kit produces five lysates where only three of the five lysates were utilized for the western blot. The procedure is as follows. First, 20-60 × 10^6

BMDC were harvested post 10 hour stimulation with 8μg/mL GC and pelleted. Ice cold cytoplasmic extraction buffer (CEB) containing protease inhibitors was then added to the pellet and incubated for 10 minutes at 4°C with gentle mixing. The sample was then centrifuged at 500g for 5 minutes and the supernatant, containing the cells' cytoplasmic contents, was then collected. Next, the ice cold membrane extraction buffer (MEB) containing protease inhibitors was then added to the pellet, vortexed for 5 seconds, and incubated for 10 minutes at 4°C with gentle mixing. The sample was then centrifuged at 3,000g for 5 minutes and the supernatant, containing the cells' membrane bound contents, was then collected. Ice cold nuclear extraction buffer (NEB) containing protease inhibitors was then added to the pellet, vortexed on high for 15 seconds, and incubated for 30 minutes at 4°C with gentle mixing. The sample was then centrifuged at 5,000g for 5 minutes and the supernatant, containing the cells' soluble nuclear contents, was then collected. In order to collect the chromatin-bound nuclear extracts, 5μL of 100mM $CaCl^2$ and 3μL of micrococcal nuclease per 100μL of room temperature NEB with protease inhibitors was used. This solution was added to the cell pellet, vortexed on high for 15 seconds, and incubated in a 37°C bead bath for 5 minutes. Post incubation, the sample was vortexed on high again for 15 seconds and centrifuged at 16,000g for 5 minutes; the supernatant was then collected. The last lysate was created derived using room temperature pellet extraction buffer (PEB) containing protease inhibitors. The PEB solution was added to the sample pellet, vortexed on high for 15 seconds, and allowed to incubate at room temperature for 10 minutes. Following incubation, the sample was centrifuged at 16,000g for 5 minutes, and the supernatant, containing the nuclear cytoskeletal proteins, was collected. All the lysates were then stored at -80°C to be later used in the western blot.

While the subcellular fractionation yields the membrane bound extracts it does not specifically isolate the lysosome: for this a lysosomal enrichment and isolation was used. The protocol and materials were derived from the Lysosome Enrichment Kit for Tissues and Cells (Thermo Fisher, Cat#89839). First, 150-200 × 10^6 BMDCs were harvested post 10 hour stimulation of with 8μg/mL GC and pelleted. Next, 800μL of lysosome enrichment reagent A supplemented with protease inhibitors was added to the cells and vortexed for 5 minutes. The solution was then allowed to incubate on ice for precisely 2 minutes then transferred to a dounce homogenizer. Approximately 30 strokes of the dounce homogenizer were performed on ice. Then 800μL of lysosome enrichment reagent B supplemented with protease inhibitors was added to halt cell lysis. The solution was inverted several times to mix then centrifuged at 500g for 10 minutes at 4°C. The supernatant was then collected and added to 500μL OptiPrep Cell Separation Media to make a final concentration of 15% OptiPrep media cell lysate solution. Using two 3.2mL thickwall polypropylene tubes (Beckman Coulter, Cat#362333), a density gradient was then formed in according to descending concentration using the solutions found in **Table 1**. The cell lysate solution as then added to the top of a density gradient and ultracentrifuged 145,000g for 2 hours at 4°C.

Post centrifugation, several bands formed in the gradient. The top band, the top 600μL was collected and 1mL of ice cold PBS was added. The solution was then vortexed for 10 seconds centrifuged at 17,000g for 30 minutes at 4°C. The supernatant was then removed, leaving behind the lysosomal pellet. To this pellet, 100 μL of 1X RIPA buffer (Millipore Sigma, Cat#20-188) containing protease inhibitors was added and incubated at room temperature for

10 minutes. The lysate was then stored at -80°C to be later used as a lysate in the western blot. **Figure 5** shows an overview of the procedure.

Table 1: OptiPrep Gradient Preparation

Gradient Percent (%)	OptiPrep Cell Separation Media (µL)	Gradient Dilution Buffer (µL)	Final Volume
17	283.3	716.7	1000
20	333.3	666.7	1000
23	191.7	308.3	500
27	450	550	1000
30	250	250	500

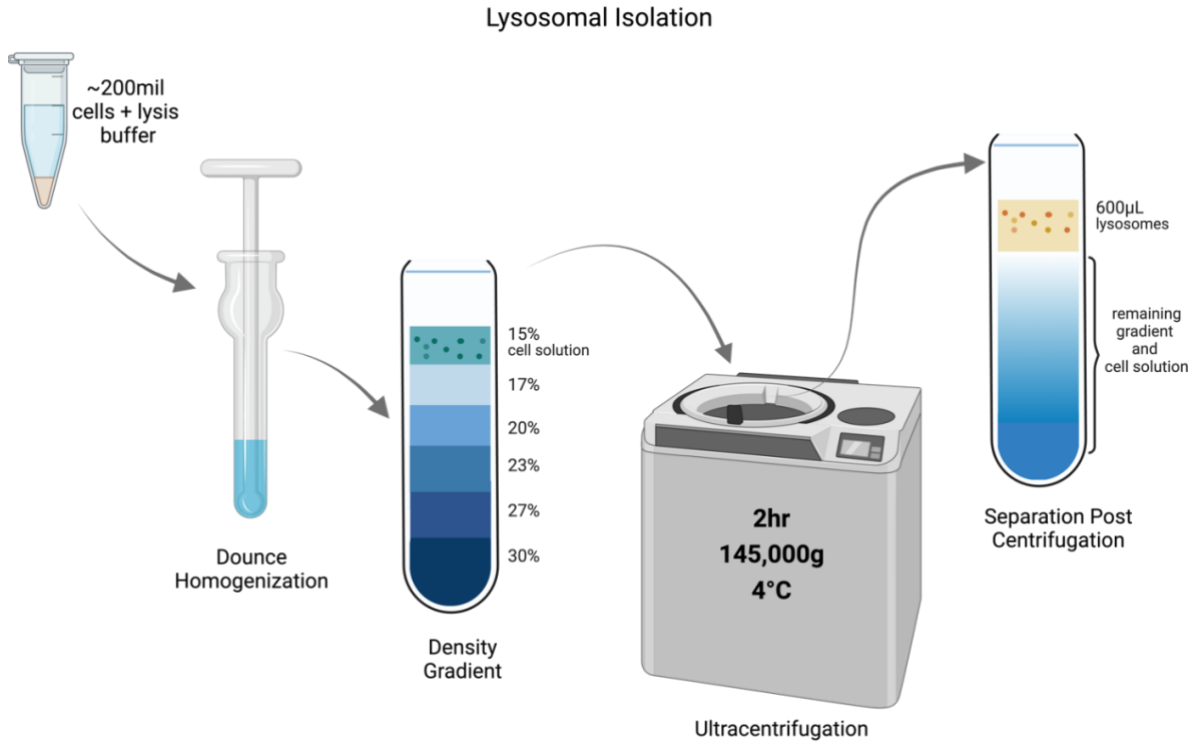

Figure 5: Lysosomal isolation procedures. The figure above depicts the process of isolating the lysosome from the primary dendritic cells. Overview the steps of adding lysis buffer to the cell pellet, using dounce homogenization as physical disruptions, adding the solution to a density gradient, and isolating the lysosomal band using ultracentrifugation.

Optimization of lysate preparation can be found in **Appendix C**.

3.3.3. Western Blot

Western blotting separates proteins based on their molecular weight through gel electrophoresis, followed by their transfer onto a membrane surface. Subsequently, the membrane is probed with specific antibodies that bind exclusively to the target protein of

interest, in this case STING. Additionally, housekeeping antibodies were utilized to confirm successful cellular fractionation within the lysates. Housekeeping proteins are controls within the procedure serving to confirm successful lysate isolations and normalize data during analysis. House-keeping proteins are used as biological controls for WB because they are constitutively expressed in different sub-cellular organelles. Antibodies were conjugated with HRP for detection via the Azure 600 Western Blot Imager.

The lysates used for the western blot include three of the five lysates extracted from the subcellular fractionation and the lysate obtained from the lysosomal isolation (seen above in chapter 3.3.2). The three lysates used from the subcellular fractionation include the cytoplasmic contents, the membrane bound contents, and the soluble nuclear extracts. **Figure 6** depicts the lysates analyzed through western blotting.

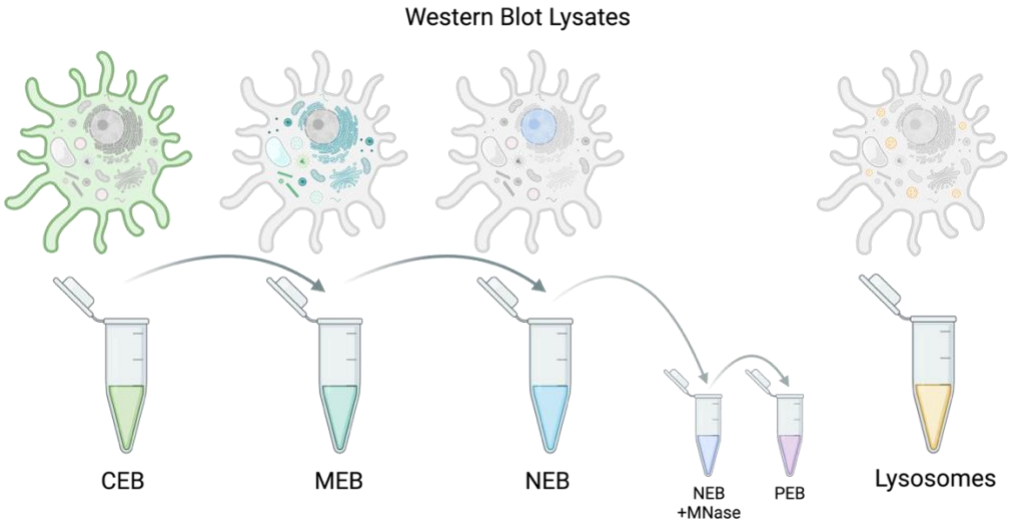

Figure 6: Lysates utilized within the western blot. Three out of five lysates created from the subcellular fractionation was used and the final lysate was derived from a lysosomal isolation. Within the subcellular fractionation: CEB= cytoplasmic extraction buffer, MEB= membrane extraction buffer, NEB= nuclear extraction buffer, NEB+ MNase= nuclear extraction buffer + micrococcal nuclease (chromatin-bound fractionation), and PEB= pellet extraction buffer (cytoskeletal proteins). The lysates derived from the NEB + NMase and PEB were not utilized within the western blot.

Prior to running the western blot, all lysates were quantified using the pierce BCA protein assay kit (Thermo Fisher, Cat#23227) and then adjusted to a final concentration of 0.5-0.75µg/µL, final concentration being dependent on starting lysate concentration. The BCA was conducted as follows. The standards were created as seen in **Table 2** using the provided stock solution of Albumin and 1X RIPA lysis buffer. The BCA working reagent (WR) was prepared at a 50:1 ration Reagent A:B using the following formula:

$$(9\ standards + \#\ unknowns) \times\ 2\ replicates\ \times\ 200\mu L = WR\ total\ volume\ (\mu L)$$

The samples were then plated on a flat bottom well plate using 10 µL of each sample/ standard and two replicates. The plate was then placed on the shaker for 30 seconds then allowed to incubate at 37°C for 30 minutes. Post incubation, the plate was allowed to cool to room temperature before the absorbance was read at 562nm on a plate reader. The results

were then analyzed through GraphPad Prism where a working range 125–2000 µg/mL was used for the assay.

Table 2: Standard Curve Preparation for BCA

Solution	Volume of 1X RIPA buffer (µL)	Albumin Standard (BSA)/ Source of BSA (µL)	Final BSA concentration (µg/mL)
A	0	300 stock	2000
B	125	375 stock	1500
C	325	325 stock	1000
D	175	175 of vial B	750
E	325	325 of vial C	500
F	325	325 of vial E	250
G	325	325 of vial F	125
H	400	100 of vial G	25
I	400	0	0

Lysates were created utilizing protein concentrations yielded from the BCA. Post protein quantification, lysates were created with a concentration of either 0.5 µg/µL or 0.75 µg/µL. Leammli Sample buffer (BioRad, cat# 1610747) was added to lysates at a 3:1 ratio and the samples were then heated at 100°C for 7 minutes to denature the proteins readying them for gel electrophoresis. Lysates were aliquoted and stored a 20°C until ready for use.

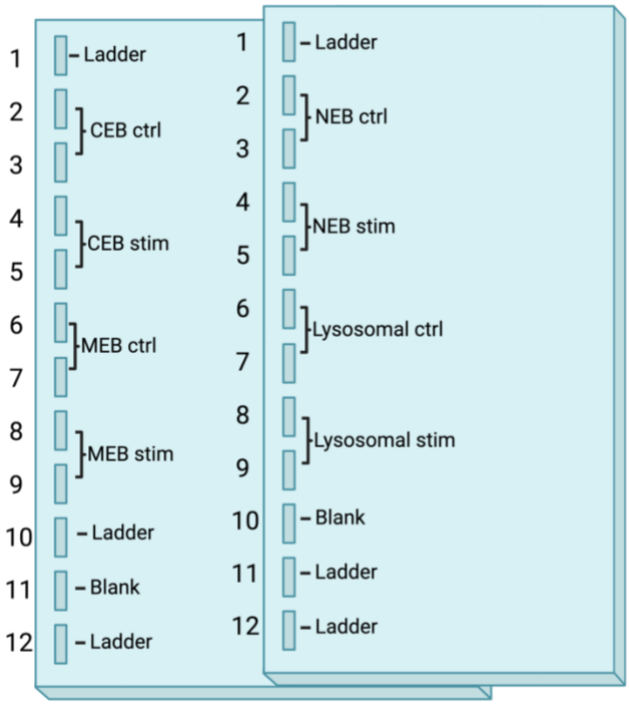

Figure 7: Western blot gel setup. The image above depicts the gel setup used for the western blot where samples and controls were run together on the same gels. A 12 well 4-12% gel was utilized and the two gels were run together in the same cassette.

The western blot gel set up was as follows. Two gels were utilized with the control and stimulated group having two replicates each. The control and experimental group for each lysate was tested within the same gel. Four lysate types and two experimental groups were utilized. The full gel setup can be seen in **Figure 7**.

Samples were run using 15μg of protein. The lysates were loaded into the gel per **Figure 7**. The gels utilized were 4-12% 12 well gels (GenScript, Cat#M00653). The gel was allowed to run in the electrophoresis chamber for 30 minutes at 60V until the samples had traveled through the stacking gel. Once the samples had made it through the stacking gel the voltage was set to 120V, and the gels were allowed to run for 1.5 hours until the samples had run to the bottom of the gel. Note that, the electrophoresis chamber was stopped before the samples ran all the way through the gel. Running buffer used was Tris-MOPS-SDS Running Buffer Powder reconstituted in 1L of Nanopure water (GenScript, Cat#M00138). Post running, the gel was set up for transfer. The transfer stack is as follows: sponge, filter paper, gel, PVDF membrane, filter paper, and sponge. The stack was encased in gel holder cassettes with the gels towards black end of the cassette and membrane towards the clear side. The cassettes were then place in the electrophoreses chamber and transfer was run for 1 hour at 100V on ice. Transfer was run in Transfer Buffer Powder reconstituted in 0.9L Nanopure water and 100mL 99% Methanol (GenScript, Cat#M00139). After transfer, the membranes were removed from the transfer stack and placed in blocking buffer for 30 minutes at room temperature. The membranes were then stained for the following proteins in the order they are listed: STING 1° Rabbit mAb (1:1000) (Cell Signaling, Cat#13647S), STING 2° Anti-Rabbit HRP (1:10,000) (Thermo Fisher, Cat#31458), HDAC2 (1:2500) (Biolegend, Cat#680105), VDAC (1:2500) (Abcam, Cat#AB185063), LAMP 1° (1:1000) (Thermo Fisher, Cat#14107182), LAMP 1 2° Anti-Rat HRP (1:5000) (NovusBio, Cat#NB7115), and Beta Actin (1:2000) (Thermo Fisher, Cat#MA5-15739-HRP). STING was the target protein while other proteins utilized served as housekeeping control staining. HDAC 2 is an enzyme primarily located in the nucleus and therefore was used as a control for the nucleic lysate [46]. VDAC 1 is the most abundant protein on the outer layer of the mitochondria and therefore was used as the housekeeping protein for the MEB lysate containing membrane bound cellular components [47]. Lysosomal associated membrane protein 1 (LAMP 1) constitutes a large portion of the lysosomal membrane making it a suitable control for the lysosomal isolate [48]. Beta Actin is largely expressed throughout the cell and is a commonly used control protein for western blotting, making it an optimal choice as the housekeeping protein for the CEB cytoplasmic cellular content lysate [49].

Primaries and HRP conjugates incubated overnight at 4°C. Secondaries were incubated for 1hr at room temperature on a shaker. Between primary and secondary staining, as well as before imaging, the membrane was washed 3 times with 0.05% PST-T for 10 minutes each wash. Between each stain the membranes were stripped using the following procedure: Nanopure water for 5 minutes, stripping buffer for 6 minutes (Advansta, Cat#R03722D50), PST-T for 5 minutes, and blocking buffer for 5 minutes. All stripping steps were done at room temperature on the shaker. Western blot imaging was conducted on the Azure 600 Western Blot Imager. For imaging, Pierce ECL Western Blotting Substrate was used for HRP detection (Thermo Fisher, Cat#32209). Results were analyzed through ImageJ and statistical analysis done on GraphPad Prism. For quantitative results, T-testing was used to test for significance.

3.4. Results

To identify the location of STING protein post GC stimulation, a western blot was utilized. This methodology was chosen as it allows for precise identification, quantification, and characterization of proteins based on their size, aiding in the elucidation of protein expression levels, post-translational modifications, and protein-protein interactions. Using this methodology both the location and relative expression levels of STING were detected in our experiments. The target protein for the western blot was the STING protein with HDAC 2, VDAC 1, LAMP 1a, and Beta Actin serving as housekeeping proteins.

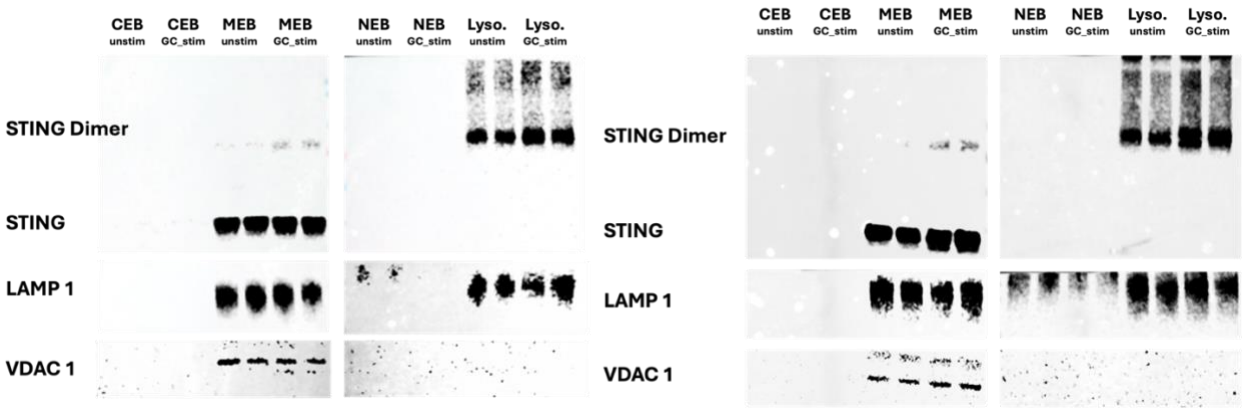

Figure 8: Qualitative results from western blotting. Demonstrates qualitative differences between GC-stimulated and non-stimulated BMDCs. Differences can be seen through dimer expression of STING. STING expression is higher in the lysosomal fraction of stimulated group compared to the control. CEB is the cytoplasmic contents, MEB is the membrane-bound cellular contents, NEB is the nucleic cellular contents, and Lyso is the lysosomal contents of the cell. LAMP 1 and VDAC 1 serve as control proteins for the lysosome and mitochondria respectively.

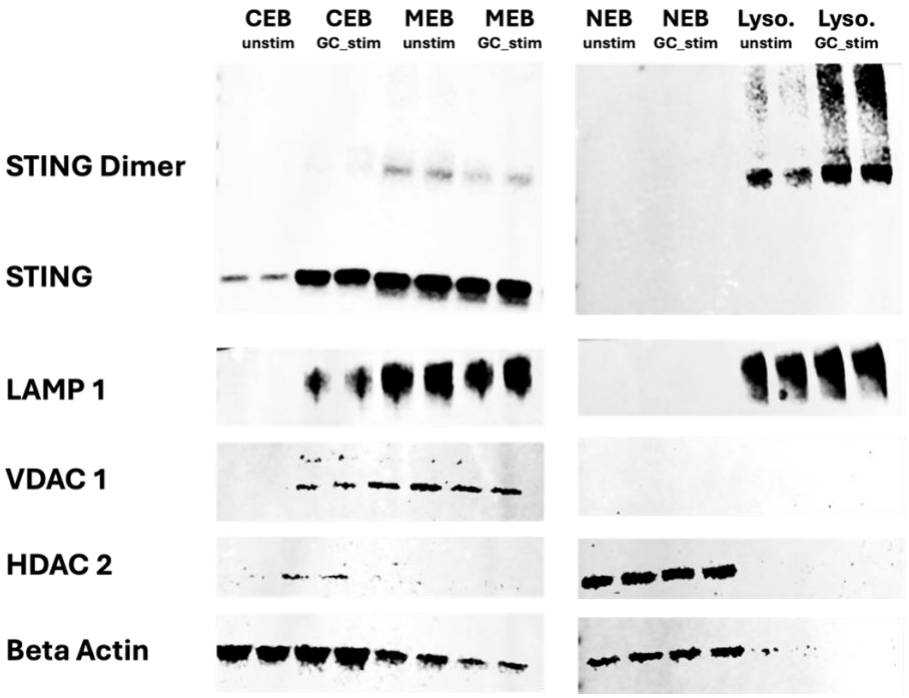

Figure 9:W*estern blot with STING expression and STING dimer expression*. *CEB is the cytoplasmic contents, MEB is the membrane bound cellular contents, NEB is the nucleic cellular contents, and Lyso is the lysosomal contents of the cell. LAMP 1, VDAC 1, HDAC 2, and Bet*a Actin served as control proteins to show that the lysate isolation for each subcellular component was successful. Note: There have been some reports of low expression of HDAC 2 in the cytoplasm, this can be seen by the slight bandage in the CEB lysates [50].

It can be seen in **Figures 8 & 9** that STING is present within the membrane and lysosomal isolations. STING in the membrane lysate can be seen at ~35kDa [51]. STING within the lysosome can be seen at ~70kDa as the protein dimerizes once activated [52]. Within the lysosomal groups STING has an increased presence within the stimulated group indicating an increased presence of STING within the lysosome upon GC stimulation. These results indicate an uptake in STING trafficking to the lysosome upon interactions with GC.

Quantitative analysis was not feasible on the samples at this time. Two factors contributed to challenges limiting quantitative analysis: upregulation of the housekeeping protein, and intensity variations dependent on exposure times. The housekeeping protein used to normalize the STING expression in the lysosomal lysate was LAMP 1. During the western blotting, it was noticed that the expression of LAMP 1 was higher in the stimulated groups than the control groups (as seen in **Figure 9)**. This led to the hypothesis that LAMP 1 was upregulated in response to GC stimulation. This was later confirmed in our bulk RNA sequencing data where in response to GC stimulation LAMP 1 is upregulated, hence the increased expression detected on the western blot (see Chapter 5 below). Additionally, while lower exposure time was able to better highlight differences between the stimulated and control group, it caused inconsistencies with data analysis. An example of this variability can be seen in **Figure 10.** Here it can be seen that a 2 second difference in exposure drastically changed the measured intensity density for the STING expression. Stimulated STING expression within the lysosomal isolate was not drastically altered as its expression was high and resistant to alterations. However, the STING expression in the control group was much lower, therefore exposure time significantly affects its appearance during imaging. This effect can be seen both qualitatively in **Figure 10** and quantitatively in **Figure 11**. In **Figure 11** it can be seen how the variance in intensity can affect whether or not the difference between the control and stimulated groups were statistically significant from one another. For this analysis, an unpaired t-test with Welch's correction was used with significance $P<0.05$.

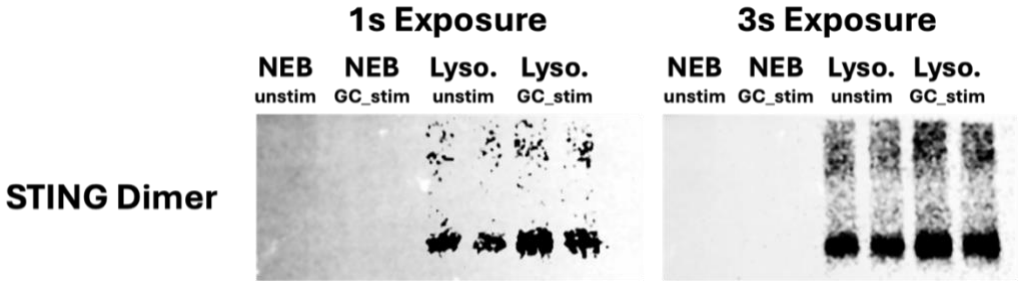

Figure 10: **Exposure time effects.** STING dimer from gel two expression variations based on exposure time. NEB is the nucleic cellular contents, and Lyso is the lysosomal contents of the cell. Differences in control group (CTRL) and stimulated group (STIM) are more apparent during ImageJ analysis in the 1s exposure group compared to the 3s exposure group.

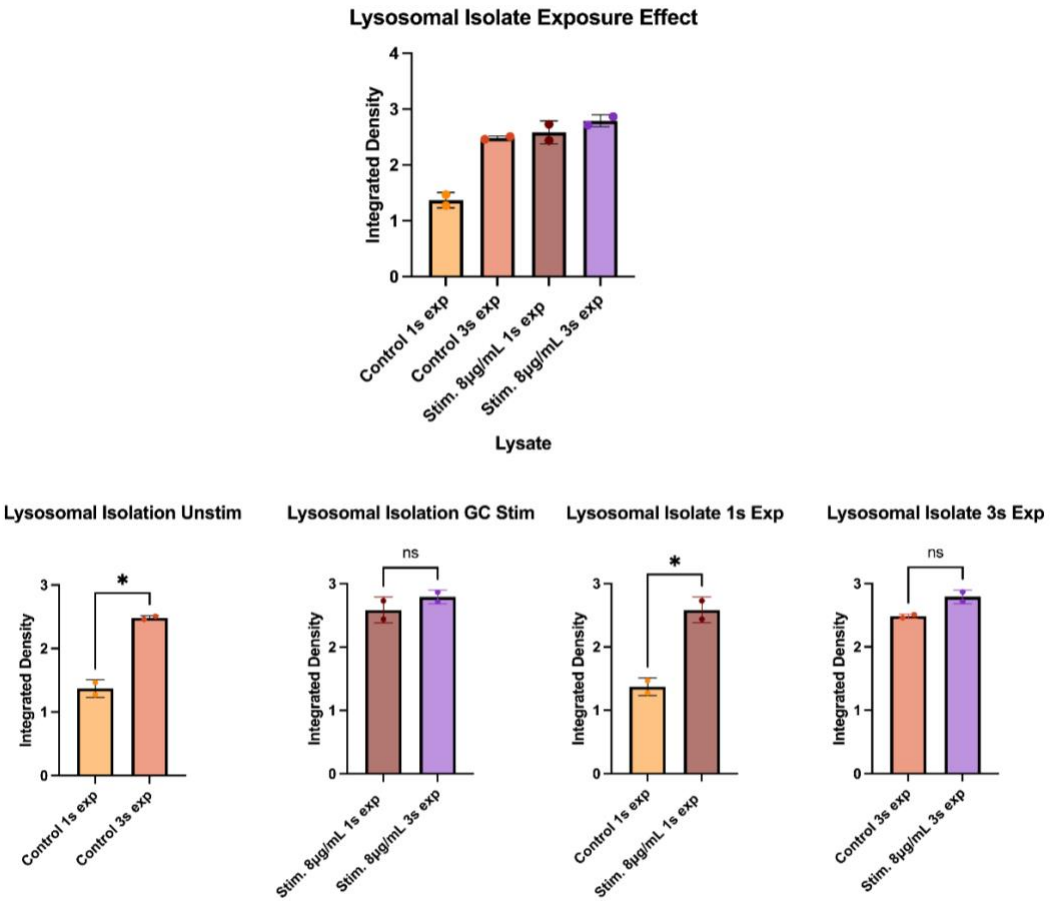

Figure 11: **STING expression vs exposure time**. Differences in detected STING expression integrated density dependent on exposure time. Changes in exposure time changes severity of data trends and whether or not significance can be found between experimental groups. Overall exposure effect is shown with changes in significance highlighted below. Significant changes seen in control (unstimulated) group between the 1s and 3s exposure times. GC stimulated band intensity not significantly affected by exposure time differences.

Due to these factors, limited quantitative analysis was able to be performed at this time. However, in order to highlight the general trend, unnormalized data was gathered. This data is the integrated intensity of the STING expression without normalization to a housekeeping protein. This data is illustrated in **Figure 12**.

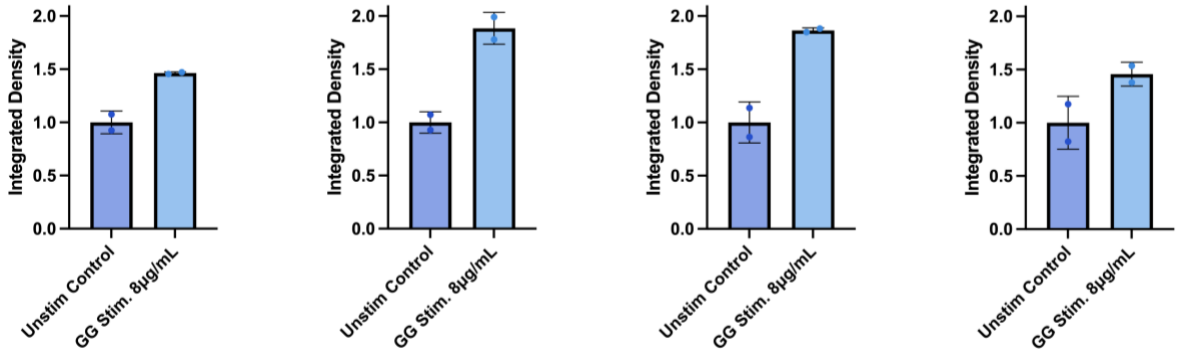

Figure 12: Western Blotting Lysosomal Isolate Integrated Intensities. The control group received no GC stimulation and the stimulated group received 8µg/mL of GC for 10 hours prior to sample collection for western blotting. A general trend can be seen here of increased STING presence in the lysosome following stimulation.

The integrated intensity data for the lysosomal isolate is presented in **Figure 12**. The purpose of this data is to demonstrate the general trend present within the lysosomal isolates. Data was normalized to the control for analysis. From this data, there is increased STING expression within the stimulated lysosomal isolate in comparison to the control unstimulated group. The results are from two biological replicates each with two technical replicates. The trend is apparent across all trials both in **Figure 12** and qualitatively in **Figures 8 & 9**. The general trend observed indicates that STING and GC are present in the lysosome at the 10 hour time point of stimulation.

Chapter 4: Cellular Swelling and Signs of Immunogenic Cell Death Post Glycated Chitosan Stimulation

4.1. Purpose

The purpose of this experimentation was to view STING and GC interactions within the lysosome via immunofluorescence antibody tagging. A previous methodology utilizing expansion microscopy can be seen in the **Appendix D**. This was not utilized as the final imaging technique due to limitations within the antibody tagging.

4.2. Materials

A GC-FITC aqueous solution (10mg/mL) was provided by ImmunoPhotonics. Male and female 8-12 weeks old C57BL/6J mice were purchased from Jackson Laboratories. Sex was varied to eliminate sex-associated immune differences and the age range 8-12 weeks was utilized as it an ideal age range for BMDC generation [42], [43].

4.3. Methods

4.3.1. Cellular Microscopy

Coverslips (18mm, #1 glass) for cell culture were utilized. Coverslips were placed in piranha solution (3:1 ratio of 95-98% sulfuric acid and 30% hydrogen peroxide) and allowed to sit for 15 minutes. Slips were then rinsed and one placed into each well of a 12 well plate. Each well was filled with PBS, treated with UV light for 10 minutes, and stored at 4°C for later use. Upon use, the plate was treated again with UV light for 10 minutes.

BMDCs were prepared according to above mention protocol, plated in a 6 well plate at a seeding density of 500 x 10^5 per plate, and stimulated for 10 hours with 8μg/mL GC-FITC. Only 8 of the 12 wells were stimulated with 4 wells were left as staining controls. Post stimulation, the well was fixed with 1 mL of 4% PFA and 0.1% glutaraldehyde in 1X PBS for 15 min at RT. Post fixation the samples were quenched to remove autofluorescence. This was done by adding a 1mg/mL solution of sodium borohydride in PBS to the samples for 10 minutes followed by a solution of 100 mM glycine in PBS incubated for 20 minutes. Post quenching the wells were rinsed 3 times with PBS. The samples were then incubated with wheat germ agglutinin (WGA) conjugated with CF®405S (1:100) (Biotium, Cat#29027-1) for 20 minutes at room temperature. Samples were then permeabilized with 0.1% (V/V) Triton X-100 for 5 minutes at room temperature. Following permeabilization, samples were washed 3 times with 1X PBS then stained with primary antibodies: STING 1° Rabbit mAb (1:200) (Cell Signaling, Cat#13647S) and LAMP 1° (1:200) (Thermo Fisher, Cat#14107182). Antibodies were allowed to incubate for 1 hour at room temperature with shaking. Post antibody incubation samples were washed 3 times for 20 minute durations with 0.1% PBS-T. Secondary antibodies were then added to samples: Cyanine5 (1:1000) (Thermo Fisher, Cat#A10525) and Alexaflour 555 (1:500) (Thermo Fisher, Cat#A32732) respectively. Post staining samples were washed 3 times for 20 minute durations with 0.1% PBS-T and left in 1X PBS until imaging. Overview of the protocol can be seen in **Figure 13**.

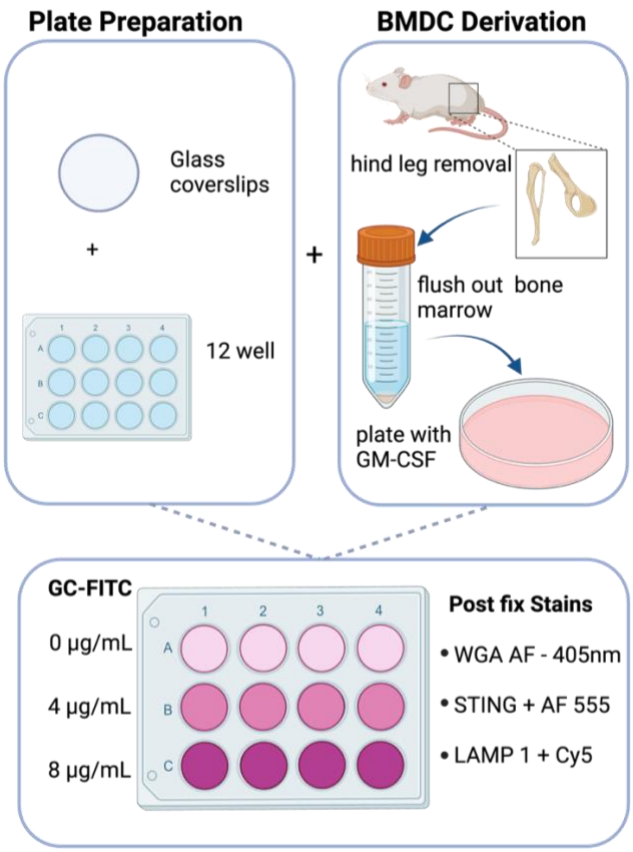

Figure 13: IF procedure on BMDC. Overview of the IF procedure for sample loading, BMDCs for plating, and plate setup for GC-FITC stimulation. Coverslips were prepped and placed in a 12 well plate. Cells were derived through hind leg extraction, retrieval on bone marrow, and plating in petri dishes. Cells were differentiated to BMDC through the addition of GM-CSF. BMDC were plated in the prepared well plates and then stimulated with GC-FITC at concentrations 0µg/mL, 4µg/mL, and 8µg/mL. Post staining samples were stained with WGA, STING-AF555, and LAMP1-Cy5 then imaged.

Post staining the samples were imaged by placing the coverslips on glass bottom dishes (35mm, #1.5H glass) using the ZEISS Laser Confocal Scanning Microscope 800 with Airyscan. This technology uses 32 honeycomb micro-lenses to enhance the resolution without increasing noise or reducing the signal [53]. The technology has each of the 32 lenses detect a small portion area of the Airy disk. The individual images from each detector are then shifted to the center position to yield one cohesive image with a 1.7 increase in resolution [54]. **Figure 14** depicts the honeycomb setup of the Airy disk and Airyscan detector.

The ZEISS 800 was used to detect signal on the 405, 488, 561, and 633nm channels. The stains utilized were WGA 405nm, GT-FITC, STING-AF555, and LAMP1-Cy5. The arrangement of their excitation and emission wavelength can be seen below in **Figure 15.** These dyes were chosen as there was enough spacing between peaks to allow for each signal to be detected without too much overlap.

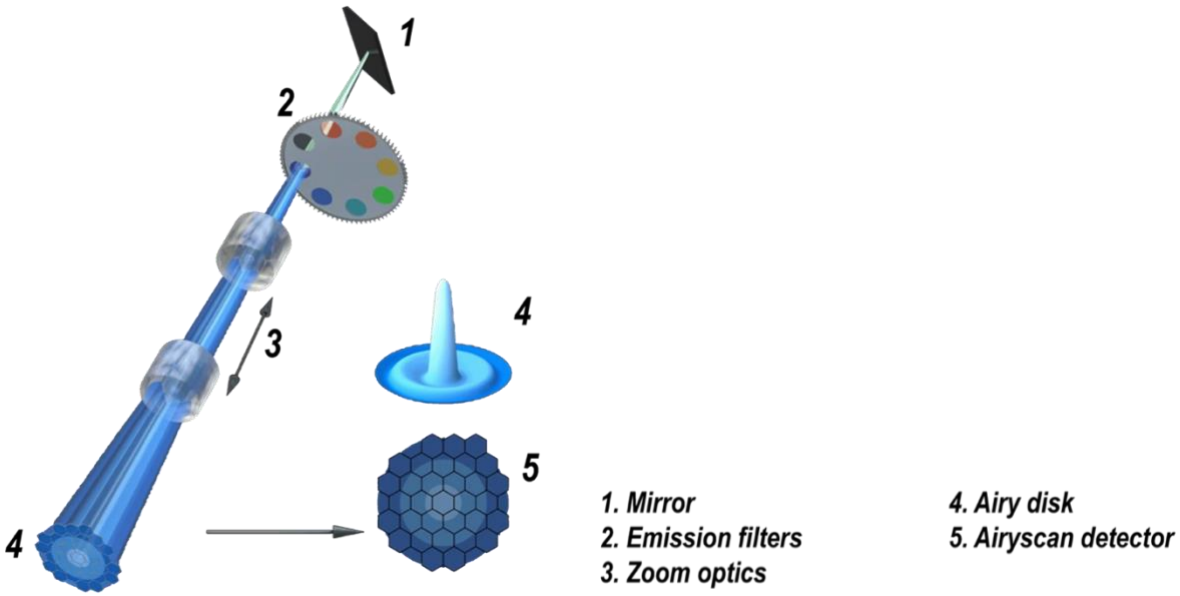

Figure 14: Setup of the Airy disk and Airyscan detector. Each component of the Airyscan setup is shown with the mirror (1), emission filter (2), zoom optics (3), Airy disk (4), and Airyscan detector (5). Shows the 32 honeycomb disk arrangement. Reproduced and modified from Huff with permission from Springer Nature [55].

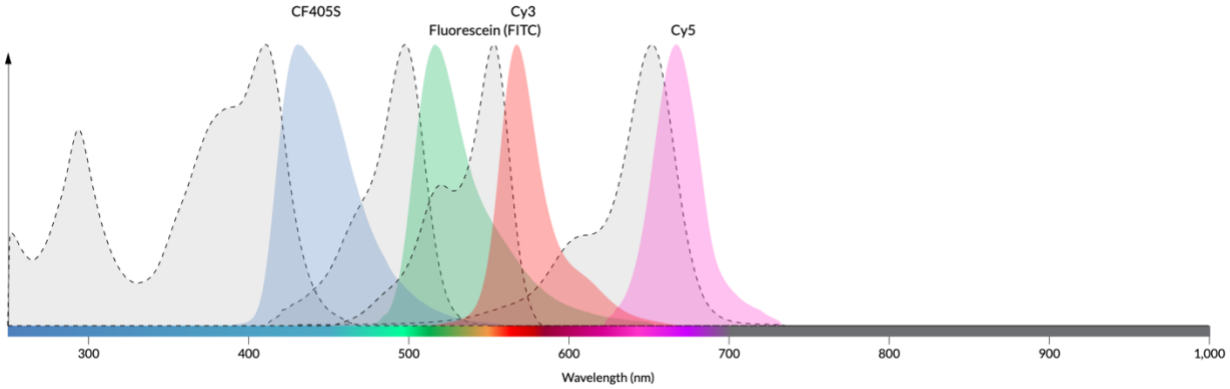

Figure 15: **Emission wavelengths of stains used in IF procedures**. Excitation and emission wavelengths of WGA 405, GC-FITC, STING-AF55, and LAMP 1-Cy5.

4.3.2. Cellular Microscopy Quantitative Analysis

In order to quantify the overlap between the GC-FITC and STING expression, ImageJ was utilized. The process for analysis is as follows. The images were loaded into ImageJ and the 488nm (FITC) and 561nm (STING) channels were analyzed. The images were set to 8bit to best mimic the capabilities of the human eye [56]. Following image type adjustments, the threshold on both channels were set to "B&W" and "Ostu." The scale was then set to pixels and measurement set to give mean signal values based on the FITC channel. The particle fluorescence of the FITC channel was then extrapolated using the particle analysis function. From this, the lowest fluorescent value was used as a threshold value. This threshold would

determine which particles of STING overlapped onto the GC-FITC particles by eliminating the STING particles whose mean grey value was too low once projected onto the FITC image. The STING particles were then overlayed with the FITC channel using the particle analysis function. From this, the fluorescent intensity of each STING particle in relation to the FITC channel was extrapolated. After the threshold was applied, the particle overlap was gathered from this data. The macro for this procedure can be seen in **Appendix E.**

4.4. Results

Immunocytochemistry was utilized to investigate colocalization of STING and GC. Fixing and staining occurred following a 10 hour stimulation period with GC-FITC. The staining illustrates STING and GC activity in relation to other subcellular components. LAMP 1 is a lysosomal associated membrane protein known to aid in the creation and fusion of autophagolysosomes [48]. It has been used in previous studies by Gaidt et al. to demonstrate colocalization between STING and the lysosomes within human myeloid cells [40]. As LAMP 1 is an integral part of lysosomal autophagy activity and has been previously used in investigations of the STING pathway, it was chosen for this study.

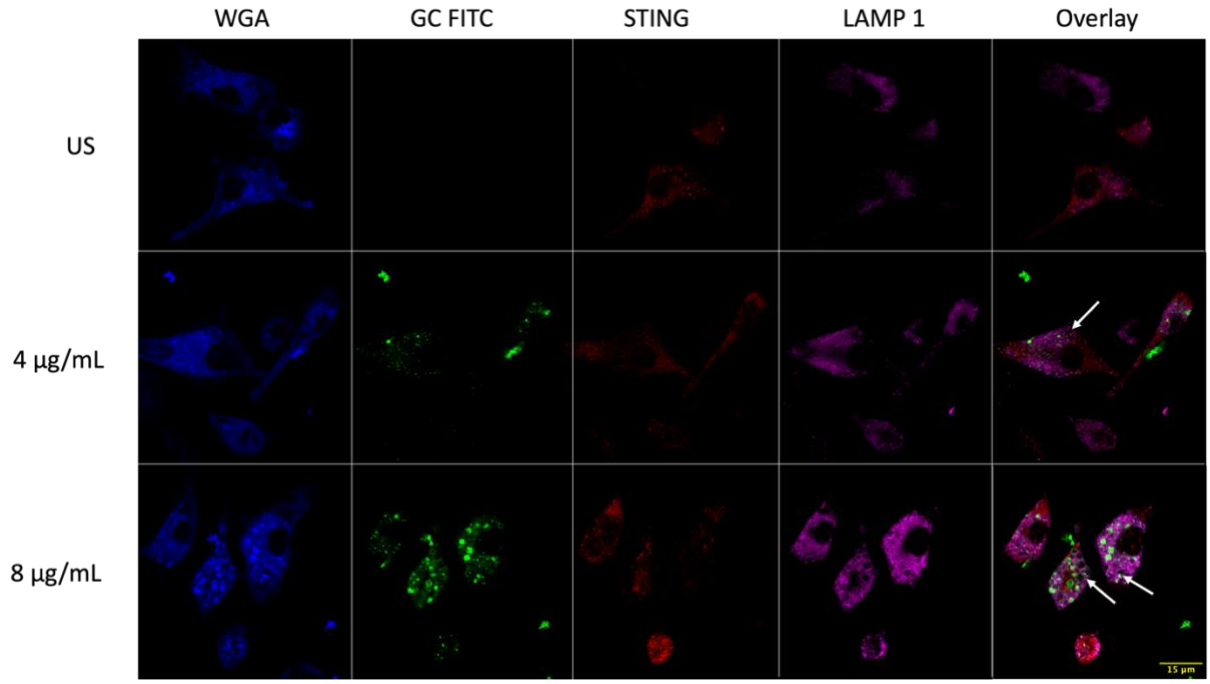

Figure 16: Airyscan images of BMDC stimulated with GC-FITC. Post fix staining tagging STING protein and LAMP-1. Overlay shows GC-FITC, STING, and LAMP 1 overlap. WGA (wheat germ agglutinin) was used to locate cells and identify cell margins. Cellular swelling can be seen in cells stimulated with GC-FITC. Arrows highlight swollen vesicles within the cells.

It can be seen that GC stimulation resulted in cellular swelling prompting the question if the overall cell volume changed as well. Upon cell size analysis no significant change was found, process and results for this analysis can be found in **Appendix F**. It is hypothesized that the intracellular organelles are swelling but this does not correlate to overall cell size increase; potentially cell size increase may be seen at a later time point when the cell is closer to cell

death. In order to gain further insight into the vesicle enlargement, ROIs were taken allowing a more detailed view of the GC-STING interactions. These ROIs can be seen below in **Figure 17.**

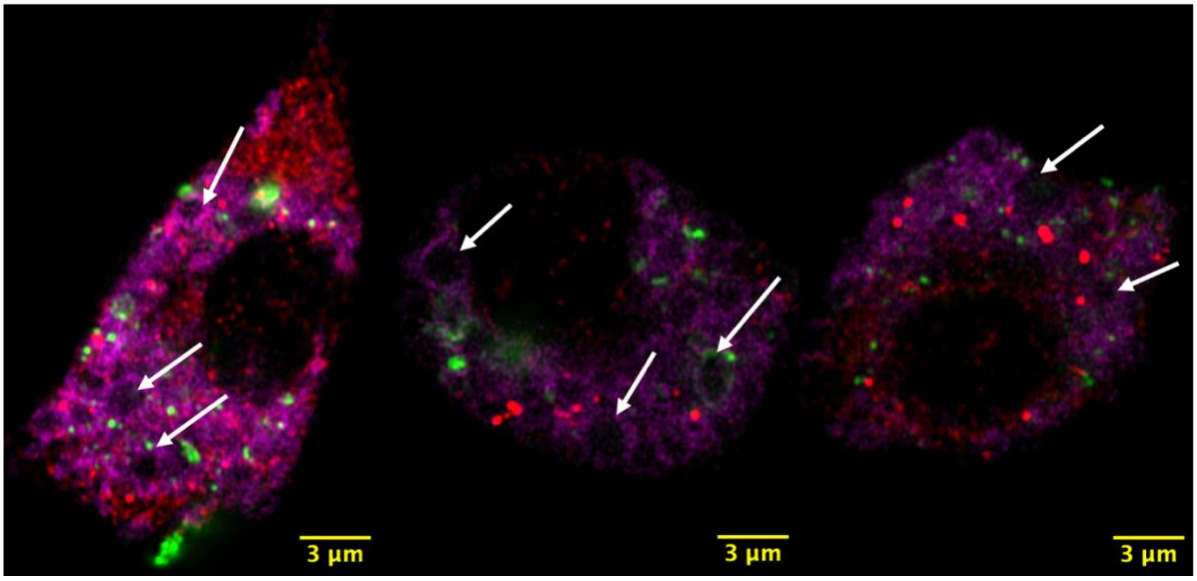

Figure 17: **Regions of interest (ROIs) showing more detail of GC-STING interactions**. STING is tagged with AF555 in red, GC is tagged with FITC in green, and LAMP 1 is tagged with Cy5 in magenta. LAAMP 1 is presumably showing lysosomal presence. Cellular swelling can be better visualized where presence of GC can be seen within some of these vesicles. Arrows highlight the swollen vesicles within the cells.

The ROIs seen in **Figure 17** serve to further highlight the GC and STING interactions. The results in **Figure 18** show that there are swollen cellular vesicles, some of which contain GC and STING expression. This indicates that GC and STING are both colocalizing within these vesicles prior to cell death.

Table 3: GC-FITC and STING Particle Overlap Analysis

Concentration (GC-FITC)	4 ug/mL			8 ug/mL		
FITC Particle Count	212	77	143	249	129	172
Overlap (FITC and STING)	15	6	17	39	38	49
STING Particle Count	988	708	647	1703	394	516
Overlap of STING on FITC	0.015	0.008	0.026	0.022	0.096	0.094
Overlap %	**1.518**	**0.847**	**2.627**	**2.290**	**9.644**	**9.496**
Overlap of FITC on STING	0.0707	0.077	0.118	0.156	0.294	0.284
Overlap %	**7.075**	**7.792**	**11.888**	**15.662**	**29.457**	**28.488**

While interactions can be seen between GC and STING, the images do not quantify the percentage of overlap between the two. In order to quantify this colocalization, analysis through ImageJ was conducted. This analysis required thresholding to be applied to both the GC-FITC and STING channels to then enumerate the particles detected. **Figure 18** shows the results of applying the threshold to each channel and the subsequent particles that were extrapolated from this analysis.

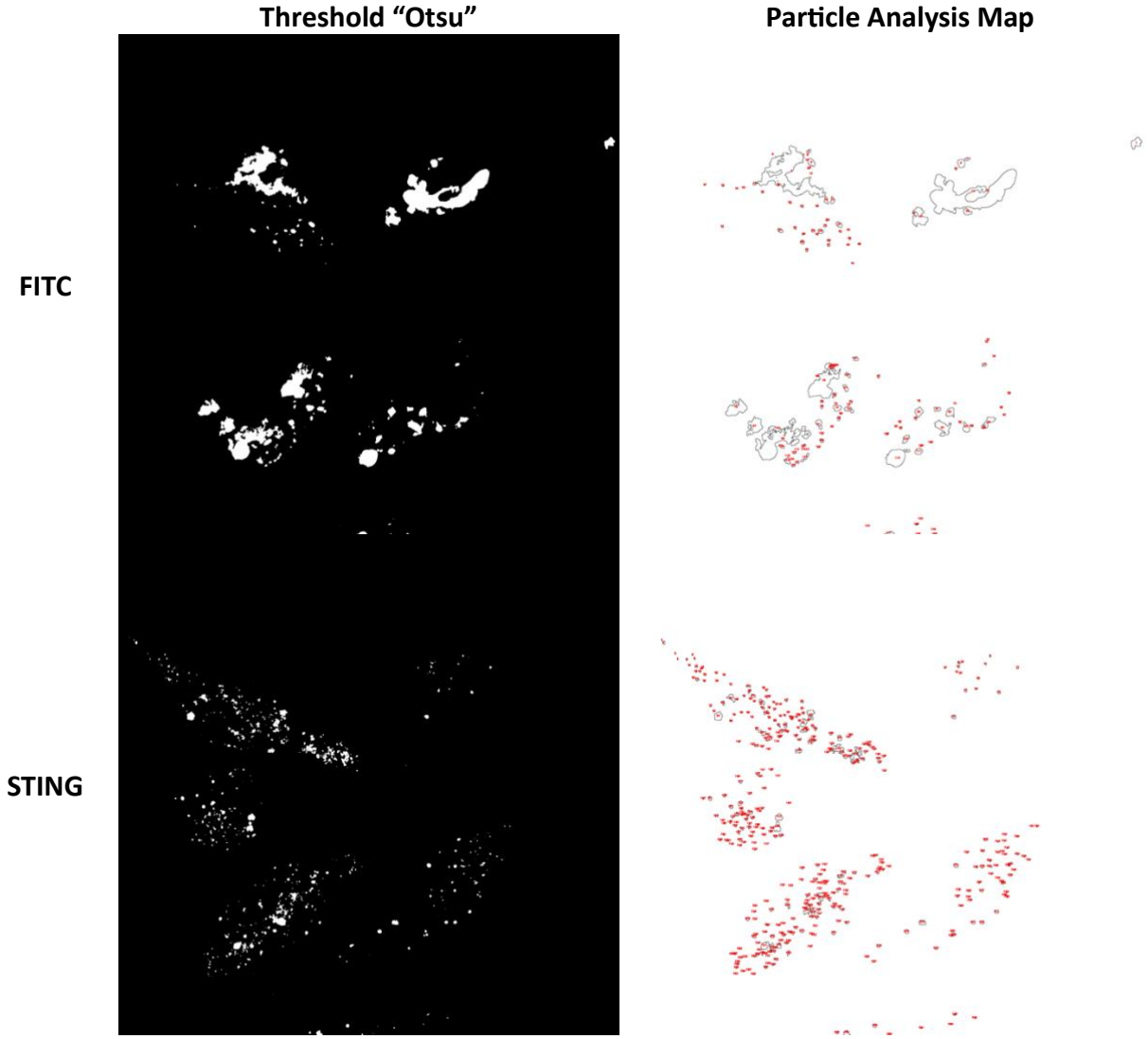

Figure 18: **Particle Analysis Procedures.** Shows the intermediate images resulting in particle overlap analysis between GC-FITC and STING. The images show how particles were detected by the imageJ program. Thresholding serves to isolate the particles based on intensities (left panels), and the particle analysis map (right panel) served to count the particles present in each channel. The FITC channel analysis provided a threshold value for STING particle mapping. Intensities recorded above this threshold indicated particle overlap.

The data for the field of view and the particle analysis are to show the overlap of FITC and STING. STING is a highly expressed protein throughout the cell; therefore, it is not expected for a majority of this protein to overlap with FITC and not all the STING within the cell will be recruited for the STING pathway upon GC stimulation. However, it is notable to look at how much of the GC that enters the cell is interacting with STING. From the data set, there is approximately 16.7% overlap of FITC on STING particles. This overlap increases slightly when looking at the 8µg/mL samples which have an average overlap of 24.5%. While there is some overlap, the percentage is not very significant in the different groups. From this, interactions can be gathered but colocalization cannot be fully established. This indicates that the 10 hour time point may not fully capture the GC-STING interactions. Single-cell analysis demonstrating similar trends can also be seen in **Appendix G.**

Chapter 5: Stimulation with Glycated Chitosan Results in an Upregulation of Lysosomal Genes and STING pathway Interactions

5.1. Purpose

The purpose of this experimentation was to utilize the bulk RNA sequencing data from prior experimentation and investigate trends between lysosomal gene expression and GC stimulation.

5.2. Materials

Aqueous solution of N-dihydrogalactochitosan, also referred to as glycated chitosan (GC), (10mg/mL) was provided by ImmunoPhotonics, Inc. Male and female 8-12 weeks old C57BL/6J mice were purchased from Jackson Laboratories.

5.3. Methods

5.3.1. RNA Sequencing (RNA-Seq)

This protocol was conducted priorly in the lab and the data preserved. The overview of sample collection is as follows. BMDCs underwent a 24-hour culture, followed by harvesting and staining with ghost dye BV510 to assess viability, as well as CD11b APC-Cy7 and CD11c FITC. Live CD11b+CD11c+ BMDCs were then isolated via sorting on the BD FACS ARIA. RNA extraction from the sorted BMDCs was accomplished using the Quick-RNA microprep kit obtained from Zymo Research (Cat# R1050) and conducted according to the manufacturer's instructions. For sequencing, mRNA preparation and sequencing service involving 20 million reads were performed to prepare the RNA for NovaSeq PE150 reads on the NovaSeq6000 platform.

5.3.2. Bioinformatics Analysis (Quality Control, Read Trimming, Genome Mapping, and Identification of Differentially Expressed Genes)

An initial quality assessment of the raw sequencing data was carried out using FastQC (v0.11.9) to identify common issues in RNA-Seq data. Subsequently, Trimmomatic (v0.39) was employed to trim the reads, eliminating low-quality bases [57]. FastQC was then used again to verify the enhancement in quality post-trimming. The RNA-Seq reads from each sample were aligned to the mouse mm10 genome assembly using HISAT2, and Samtools was utilized to convert the HISAT2-generated SAM files into BAM files [58]. The Subread package's FeatureCounts program was employed to quantify the mapped RNA-Seq reads for genomic features [59]. DESeq2, based on the negative binomial distribution, was utilized for the analysis of differentially expressed genes (DEGs). The resulting P-values underwent adjustment utilizing the Benjamini and Hochberg's approach to control the false discovery rate. Genes exhibiting an adjusted P-value (P adj) < 0.05 as determined by DESeq2 were categorized as differentially expressed. Furthermore, Gene Ontology (GO) analysis of DEGs was conducted using clusterProfiler [60].

5.4. Results

Literature research was conducted to find genes associated with lysosomal activity and cell death. Additional genes were added to the list from NIH database with the search “lysosome death” AND "Mus musculus" [61]. These search criteria encapsulate both gene function and mouse strain. The relative expression for these genes was then shown for both GC stimulated and unstimulated groups of both wild type and STING knockout cells. The resulting heatmaps can be seen below in **Figure 19.**

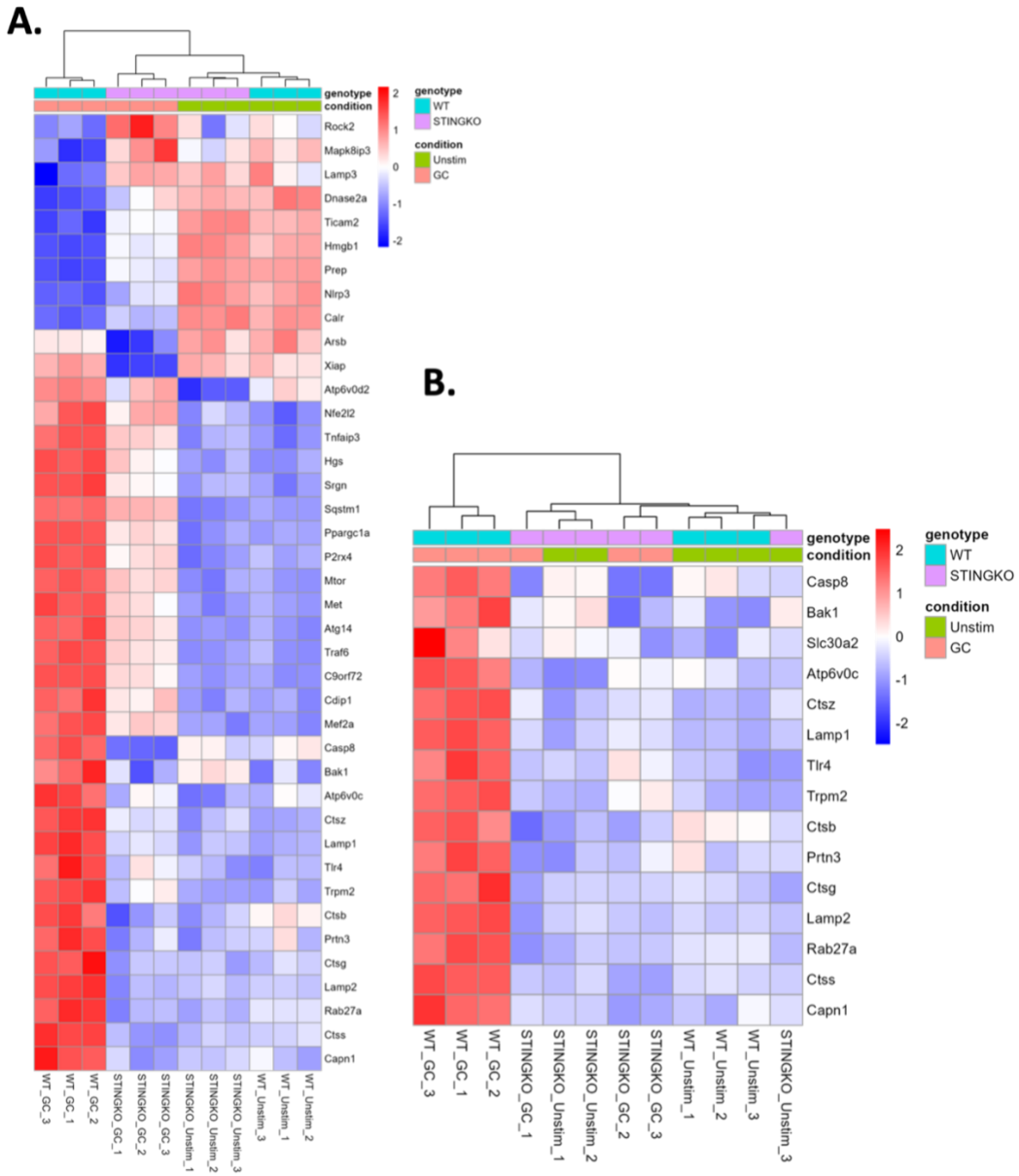

Figure 19: Lysosomal gene heatmapping. Heatmaps illustrating activity of lysosomal and cell death-associated genes in relation to STING pathway activity. In panel A, genes expression associated with cell death and lysosomal death is presented. In panel B, genes upregulated by GC stimulation correlating to STING pathway activity can be seen. Both the heatmaps in panels A and B show both STING knockout (KO) and wild type (WT) genotype groups with conditions of unstimulated (unstim) and GC stimulated (GC). The expression levels of this genes can be seen with dark red illustrating upregulation and dark blue illustrating downregulation.

The upregulation of genes associated with the lysosomal death and NLRP3 pathway seen in **Figure 19** prompted further analysis. Genes directly associated with the NLRP3 pathway were gathered and the bulk RNA sequencing data investigated for trends within the gene expression. The list of genes was compiled through literature research and NIH database gene search “NLRP3 inflammasomes pathway” AND "Mus musculus” [62]. Results of this investigation can be seen below in **Figure 20.**

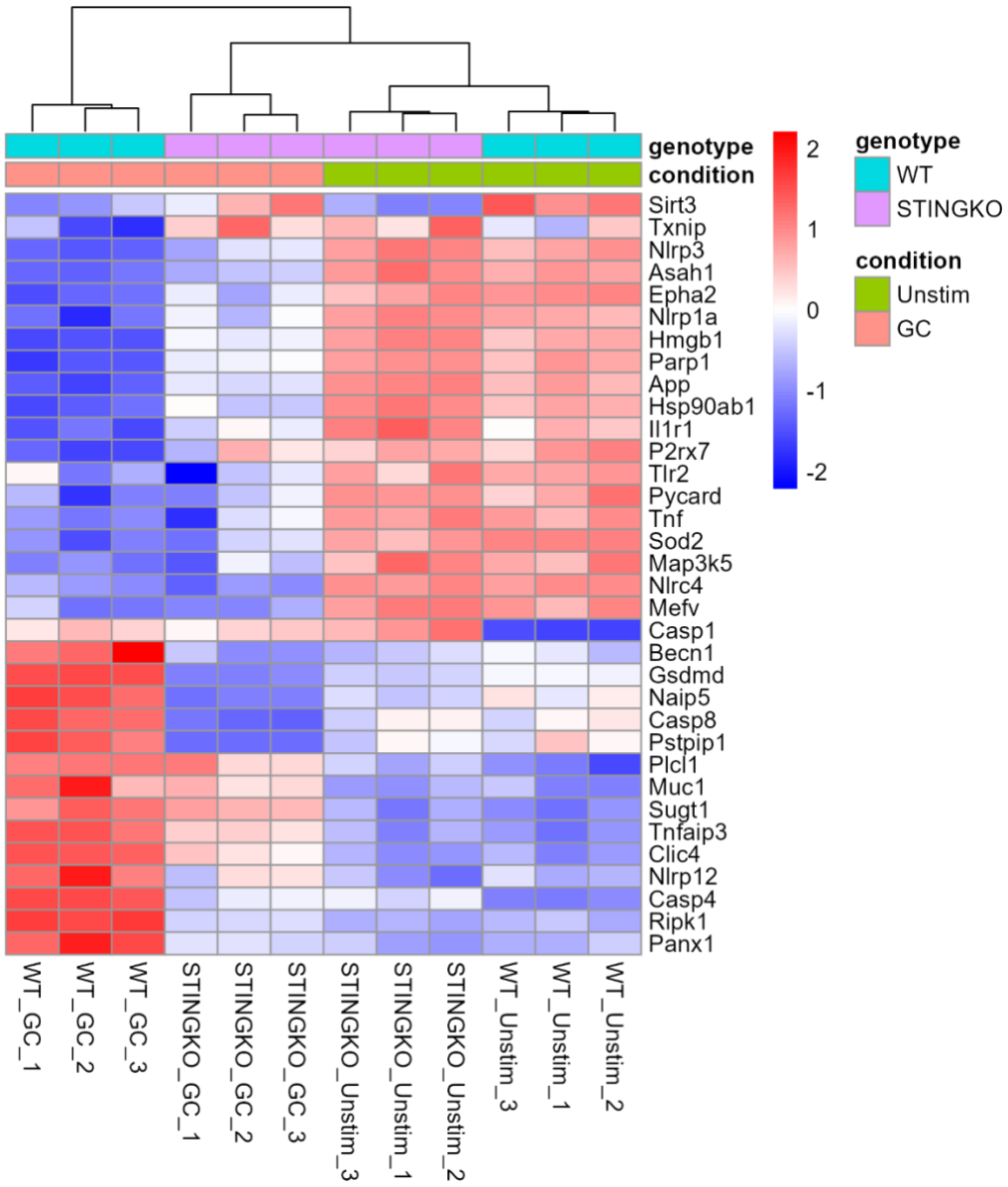

Figure 20: **NLRP3 pathway heatmapping**. Heatmap illustrating genes known to be associated with the NLRP3 pathway. The data presented includes both STING knockout (KO) and wild type (WT) genotype groups with conditions of unstimulated (unstim) and GC stimulated (GC). The expression levels of this genes can be seen with dark red illustrating upregulation and dark blue illustrating downregulation.

5.5. Key Gene Discussion

In **Figure 19**, genes associated with "lysosomal activity" and "cell death" were presented. Panel B shows further analysis, isolating the genes that correlate to STING pathway activity. These genes are associated with cell death and are only upregulated in the presence of STING pathway activation. Among the listed genes in Figure 21 (B), caspase 8 is upregulated. Caspase 8 is known to be upregulated in STING-mediated apoptosis and pyroptosis but downregulated in STING 1 necroptosis [63]. Once Caspases 8 and 10 are activated, they trigger the caspase activation cascade which mediates programmed apoptotic death [64]. Cui et al. found that in macrophages, the infection by *Mycobacterium bovis* (*M. bovis*) activated the STING-TBK1-IRF3 pathway resulting in apoptosis following interactions with Bax and caspase-8/caspase-3 [65]. It is also related to GSDMD cleavage, a key step in the NLRP3 pathway in STING1 pyroptosis [63, p. 1]. When STING engages the lysosomal death program it is known to engage NLRP3 [66]. Caspase 8 is an indicator of this pathway activation. Additionally, Cathepsin B (Ctsb), Cathepsin s (Ctss), Cathepsin G (Ctsg), and Transient receptor potential melastatin 2 (Trpm 2) (all connected to the NLRP3 pathway) are upregulated. Ctsb is a bidirectional regulator that balances lysosome biogenesis and autophagy. This balance determines if the NLRP3 pathway is activated [67]. Additionally, Ctsb is thought to be the main active protease after lysosomal membrane permeabilization, making it an integral molecule within the lysosomal cell death pathway [68]. Ctss is often upregulated within the NLRP3 pathway as can compensate for the loss of other cathepsins [67]. Ctsg is connected to cellular pyroptosis and has been linked to the development of pyroptosis through cleaving GSDMD into GSDMD-N (active players in the NLRP3 pathway) [69]. Trpm 2 is linked to pathways that activate NLRP3 [70]. Tseng et al., demonstrated in their study that Trpm 2-mediated Ca^{2+} influx directly leads to NLRP3 inflammasome activation.

Many genes associated with lysosomal cell death are being upregulated. Proteinase 3 (Prtn3) is being upregulated and correlates with the STING pathway. This gene is coded during lytic cell death mechanisms (pyroptosis) [71]. It has known associations with lysosomal-dependent cell death [68]. Additionally Calpain1 (Capn 1) is being upregulated by GC stimulation and has been more recently connected to the release of cathepsins and lysosomal membrane permeabilization [72].

In terms of overall lysosomal activity several key genes are being upregulated. The first to note is Atp6v0c which is involved in the encoding for ATPase (V-ATPase) [73]. This enzyme is known to be involved in both STING degradation, cell organelle acidification [74]. Cathepsin Z (Ctsz) is also upregulated; it is a lysosomal cysteine protein that is active in immune defense. Present in activities such as phagocytosis, cell-cell communication, and migration of APCs such as dendritic cells [75]. Recent studies have linked Ctsz to the NLRP3 pathway, however, the exact pathways still remain unclear [67]. Lysosomal-associated membrane protein 2 (Lamp 2) is unregulated; this protein is associated with membrane formation of the lysosome with recent connections to cell death and autophagy [76]. Overall, its upregulation shows an increase in lysosomal activity. Alongside this, lysosomal-associated membrane protein 1 (Lamp 1) is upregulated. Structurally similar to Lamp 2, Lamp 1 is known to be associated with increased lysosomal activity and is linked to the STING pathway during STING trafficking and degradation in the lysosome [76],[77].

In our experiments, the heatmaps in **Figure 19** show the upregulation of these genes associated with both the STING pathway and lysosomal-induced death is an indicator that GC plays an active role in these pathways. Many of these genes are associated with the NLRP3, as previously mentioned, and have been shown to have cross-talk with the STING pathway. For further analysis, genes associated with the NLRP3 pathway were collected and data shown in the heatmap seen in **Figure 20**.

Within **Figure 20**, the bottom portion of the heatmap is of particular interest. Within this section an upregulation of genes dependent on the STING pathway and GC stimulation can be seen. These genes include: Casp1, Becn1, Gsdmd, Naip5, Casp8, Pstpip1, Plcl1, Muc1, Sugt1, Tnfaip3, Clic4, Nlrp12, Casp4, Pipk1, Panx1. Genes of key importance to note are Casp1, Gsdmd, and Casp8. Caspase-1 (Casp1) and gasdermin D (Gsdmd) are integral to the NLRP3 pathway, with Casp1 serving as the effector within the pathway [78]. When the NLRP3 is activated, Casp1 activates and cleaves Gsdmd which forms pores in the cell membrane leading to pyroptosis [70]. Casp8, as previously mentioned, is an active player in the STING pathway. Additionally, Casp8 is known to play a pivotal role in the activation of inflammasomes within the TLRP3 pathway [79].

While the abovementioned genes are integral to the NLRP3 pathway, many other genes contribute to inflammasome activation. Tnfaip3 is shown to help regulate the NLRP3 pathway through its interactions with Tlr4 [80]. In a recent study by Luo, et. al., Plcl1 was shown to regulate NLRP3 inflammasomes in fibroblast-like synoviocytes [81]. Small glutamine-rich tetratricopeptide repeat-containing protein 1 (Sugt1) has been identified as a NLRP3 regulatory protein [82]. The upregulation of these genes illustrates the activation of the NLRP3 pathway and indicates crosstalk between GC stimulation, the STING pathway, and NLRP3 inflammasome formation.

Chapter 6: Discussion, Conclusions, and Future Directions

6.1. Discussion

The STING pathway is an integral part of dendritic cell-mediated anti-tumor response. It is a complex pathway with many different downstream processes that have overlapping mechanisms. Identifying GC's interactions with this mechanism helps to elucidate GC's overall cellular mechanism. The goal of this study was to confirm GC and STING interactions within the lysosome. This will serve as the first step to confirming the hypothesis that GC leads to immunogenic cell death through lysosomal leakage mediated by the NLRP3 pathway.

Through the western blot results an increased presence of STING in the lysosome can be detected post stimulation with GC. This can be seen in **Figure 8** and **Figure 9** where the STING expression bands within the lysosomal isolates are larger and have greater intensity within the stimulated group compared to the control group. Within the other lysates STING expression is not greatly affected by stimulation as STING within these subcellular locations does not participate in the anti-tumor response. When STING engages in its antitumor response it dimerizes and relocates from the endoplasmic reticulum (ER), hence why primary detection of STING activation was seen within the lysosomal isolate [83]. This increased expression within this lysate demonstrates that GC is interacting with the STING pathway and resulting in STING trafficking to the lysosome for further downstream processing. While this trend of increased expression can be detected it cannot be quantitively analyzed. For this analysis, a housekeeping protein not involved in this pathway will have to be utilized. Additionally, exposure times have a great impact on integrated intensity detection as seen in **Figure 10** and **Figure 11**. This further skews the quantitative analysis. In **Figure 12**, western blot band intensity differences illustrate the increased expression of STING within the stimulated group compared to the control within the lysosomal isolate. This further illustrates the hypothesis that GC induces STING trafficking to the lysosome.

In **Figure 16**, GC and STING interactions were detected. This can be seen through their colocalization within swollen cellular vesicles. These interactions can be further seen in the ROIs seen in **Figure 15**. While interactions between the two were visualized, it is necessary to quantify the amount of overlap. Image analysis shown in **Table 3** shows that overlap between GC and STING was at an average of 16.7% for both stimulation concentrations meaning 16.7% of the total GC found in the cell was overlapping with STING molecules. For the 8μg/mL stimulation group this average overlap was higher at 24.5%. While there is detectable overlap, the percentage is not very high indicating testing of a different time point might be more optimal to observe the GC-STING interactions. For future analysis, both the 8-hour and 12-hour time points, as well as higher concentration of GC, should be tested. Further adjustments can be made after particle overlap analysis on these time points is conducted. The cellular swelling observed in **Figure 16** is an indicator of cell stress which is hypothesized to be a precursor of immunogenic cell death and shows that GC is integral in inducing this cellular response. These swollen vesicles are hypothesized to be autophagosomes which are an active step within lysosomal cell death and the NLRP3 pathways. These swollen vesicles can particularly be seen in the 8μg/mL stimulation group, but smaller vesicles can also be seen within the 4μg/mL stimulation group. These finding are congruent with prior studies by Gui, et. al. where the formation autophagosomes following STING pathway activation was demonstrated [84]. In this

study, the vesicles were confirmed to be autophagosomes through electron micrographs. Moving forward, this would be a beneficial procedure to add to the analysis as confirming the NLRP3 pathway and STING-mediated cell death.

Further evidence supporting lysosomal activity and mediated cell death are the heatmaps in **Figure 19.** The genes were gathered from the NIH database using the key term "lysosomal death" and through literature research. The list was compiled and heatmaps were generated, cross referring genes associated with the STING pathway. The heatmap data shows the activation of key lysosomal-associated genes. The activation of these genes was shown to be dependent on GC stimulation and associated with the STING pathway. Many of the genes that are upregulated by GC stimulation are associated with lysosomal activity and immunogenic cell death. This helps to illustrate the type of cell death occurring post GC stimulation and gives insights into the pathways occurring. Given the genes shown are STING dependent it also gives evidence to the immunogenic cell death being STING-dependent. This supports the overarching hypothesis that the NLPR3 pathway is activated through STING-GC interactions, resulting in lysosomal cell death. Upregulation of Ctsb, Ctss, Ctsg, and Trpm 2 are also indicative of NLRP3 pathway involvement. The bulk RNA sequencing data sheds light on the mechanisms in play and is indicative of GC and STING interactions within the lysosome (**Figure 19**).

Investigating the crosstalk between NLRP3 pathway and GC stimulation further, **Figure 20** highlights gene expression associated with these pathways. The upregulation of Casp1 and Gsdmd indicated activation of the NLRP3 pathway due to STING stimulation as these molecules are key playing in NLRP3-mediated pyroptosis. Looking at both **Figure 19** and **Figure 20** it can be seen that Caspase 8 (Casp8) and Toll-like receptor 4 (TLR4) are both upregulated by the presence of GC. This further indicates that GC stimulation is linked to downstream activation of the NLRP3 pathway as Casp8 has been shown to cause the TLR4-mediated activation of inflammasomes leading to cell death [79]. The NLRP3 inflammasome formation can be separated into two distinct signaling stages: priming and activation [85]. During priming the transcriptional upregulation of NLRP3 occurs. After this, a secondary stimulus initiates activation leading to inflammasome complexes. GC could be serving as the secondary stimulus within this pathway as the genes associated with activation stage are being upregulated by GC. Genes associated with the priming stage such as Nlrp3 are downregulated which warrants further investigation. A recent study by Gritsenko, et. al. has shown that the priming may be dispensable for NLRP3 activation and instead can occur from K^+ efflux supporting the hypothesis that GC initiates this mechanism [86].

6.2. Conclusions

Work has been done to identify STING and GC interactions within the lysosome. Several procedures have been used and the results indicate these interactions (**Figures 9, 12, 17, and 19**). The western blot results show an increased STING presence in the lysosome (**Figures 9-12**), IF shows GC and STING interactions (**Figures 16-18**), and bulk RNA sequencing data shows an upregulation of lysosomal STING dependent and NLRP3 pathway associated genes in response to GC stimulation (**Figures 19 and 20**). Our study helps elucidate GC's cellular mechanism which will help to improve GC therapeutic applications and efficacy in future cancer treatments. The question becomes now, does GC cause autophagosome swelling and leakage which in turn

activates STING or does STING traffic to the autophagosome to initiate autophagosome swelling by interacting with GC? Future work will be done to investigate this question.

6.3. Future Directions

The current work indicates GC-STING interactions and NLRP3 pathway crosstalk. While work has been done to shed light on potential GC-STING interactions, more procedures can be done to mitigate some of the issues addressed in the current investigation. While western blotting and IF were indicative of STING and GC interactions within the lysosome, some future studies as outlined below are needed to fully understand the STING-GC interactions.

Different time points need to be investigated. While the 10 hour time point provided a good starting point, the 8 and 12 hour time points also need to be tested in order to better investigate GC-STING interactions. The IF imaging showed some colocalization of GC and STING at the 10 hour point the interactions may be better detected at different stimulation durations. Building on this, using electron micrograph could help to confirm autophagosome formation. This method of autophagosome confirmation was successfully utilized by Gui et. al., and would be beneficial in outlining the mechanism of cellular stress that GC induces [84].

Investigating different housekeeping proteins for the Western blotting analysis. At this time, no housekeeping protein has been found that is not simultaneously upregulated by this pathway. However, future research may reveal another protein which may be used to normalize the data.

Once the GC-STING interactions are further confirmed, steps can be taken to better illustrate these interactions. First being, isolating which STING pocket GC binds to. This can be accomplished through competitive binding assays. Next, investigations are needed to further delineate STING trafficking through the subcellular components. Additionally, immunogenic cell death via the lysosomal leakage due to STING and NLP3 pathway activation needs to be confirmed. At this moment it is clear that GC has interactions with both these pathways but the extent of which remains unclear. Further outlining the link between GC and these pathways is the next step in understanding the GC mechanism within the immune system.

References

[1] "Immunostimulant - an overview | ScienceDirect Topics." Accessed: Mar. 04, 2024. [Online]. Available: https://www.sciencedirect.com/topics/pharmacology-toxicology-and-pharmaceutical-science/immunostimulant

[2] E. F. McCarthy, "The Toxins of William B. Coley and the Treatment of Bone and Soft-Tissue Sarcomas," *Iowa Orthop. J.*, vol. 26, pp. 154–158, 2006.

[3] "Immunological Adjuvant - an overview | ScienceDirect Topics." Accessed: Jan. 07, 2024. [Online]. Available: https://www.sciencedirect.com/topics/medicine-and-dentistry/immunological-adjuvant

[4] S. S. Moni *et al.*, "Advancements in Vaccine Adjuvants: The Journey from Alum to Nano Formulations," *Vaccines*, vol. 11, no. 11, p. 1704, Nov. 2023, doi: 10.3390/vaccines11111704.

[5] D. Christensen, "Vaccine adjuvants: Why and how," *Hum. Vaccines Immunother.*, vol. 12, no. 10, pp. 2709–2711, Aug. 2016, doi: 10.1080/21645515.2016.1219003.

[6] "Adjuvants and Vaccines | Vaccine Safety | CDC." Accessed: Jan. 07, 2024. [Online]. Available: https://www.cdc.gov/vaccinesafety/concerns/adjuvants.html

[7] "Immunological Adjuvant - an overview | ScienceDirect Topics." Accessed: Jan. 09, 2024. [Online]. Available: https://www.sciencedirect.com/topics/medicine-and-dentistry/immunological-adjuvant

[8] admin, "Challenges and State of the Art: The advanced stage patient," memoinOncology. Accessed: Mar. 10, 2024. [Online]. Available: https://memoinoncology.com/preceptorship-cologne-2018/challenges-and-state-of-the-art-the-advanced-stage-patient/

[9] "What Is Cancer? - NCI." Accessed: Oct. 03, 2023. [Online]. Available: https://www.cancer.gov/about-cancer/understanding/what-is-cancer

[10] A. I. Riggio, K. E. Varley, and A. L. Welm, "The lingering mysteries of metastatic recurrence in breast cancer," *Br. J. Cancer*, vol. 124, no. 1, pp. 13–26, Jan. 2021, doi: 10.1038/s41416-020-01161-4.

[11] "Surgery for Cancer - NCI." Accessed: Mar. 12, 2024. [Online]. Available: https://www.cancer.gov/about-cancer/treatment/types/surgery

[12] "How chemotherapy works." Accessed: Mar. 12, 2024. [Online]. Available: https://www.cancerresearchuk.org/about-cancer/treatment/chemotherapy/how-chemotherapy-works

[13] W. A. Hall *et al.*, "Magnetic resonance linear accelerator technology and adaptive radiation therapy: An overview for clinicians," *CA. Cancer J. Clin.*, vol. 72, no. 1, pp. 34–56, 2022, doi: 10.3322/caac.21707.

[14] F. S. Hodi *et al.*, "Improved Survival with Ipilimumab in Patients with Metastatic Melanoma," *N. Engl. J. Med.*, vol. 363, no. 8, pp. 711–723, Aug. 2010, doi: 10.1056/NEJMoa1003466.

[15] "Cancer immunotherapy comes of age | Nature." Accessed: Mar. 12, 2024. [Online]. Available: https://www.nature.com/articles/nature10673

[16] D. S. Chen and I. Mellman, "Oncology meets immunology: the cancer-immunity cycle," *Immunity*, vol. 39, no. 1, pp. 1–10, Jul. 2013, doi: 10.1016/j.immuni.2013.07.012.

[17] C. M. Weiss *et al.*, “N-dihydrogalactochitosan reduces mortality in a lethal mouse model of SARS-CoV-2,” *PLOS ONE*, vol. 18, no. 8, p. e0289139, Aug. 2023, doi: 10.1371/journal.pone.0289139.
[18] A. El-Hussein, S. S. K. Lam, J. Raker, W. R. Chen, and M. R. Hamblin, “N-dihydrogalactochitosan as a potent immune activator for dendritic cells,” *J. Biomed. Mater. Res. A*, vol. 105, no. 4, pp. 963–972, Apr. 2017, doi: 10.1002/jbm.a.35991.
[19] J. Ding and Y. Guo, “Recent Advances in Chitosan and its Derivatives in Cancer Treatment,” *Front. Pharmacol.*, vol. 13, p. 888740, Apr. 2022, doi: 10.3389/fphar.2022.888740.
[20] S. Song, F. Zhou, R. E. Nordquist, R. Carubelli, H. Liu, and W. R. Chen, “Glycated chitosan as a new non-toxic immunological stimulant,” *Immunopharmacol. Immunotoxicol.*, vol. 31, no. 2, pp. 202–208, Jun. 2009, doi: 10.1080/08923970802629593.
[21] J. Banchereau and R. M. Steinman, “Dendritic cells and the control of immunity,” *Nature*, vol. 392, no. 6673, pp. 245–252, Mar. 1998, doi: 10.1038/32588.
[22] Q. Xiao and Y. Xia, “Insights into dendritic cell maturation during infection with application of advanced imaging techniques,” *Front. Cell. Infect. Microbiol.*, vol. 13, Mar. 2023, doi: 10.3389/fcimb.2023.1140765.
[23] L. Hato *et al.*, “Dendritic Cells in Cancer Immunology and Immunotherapy,” *Cancers*, vol. 16, no. 5, p. 981, Feb. 2024, doi: 10.3390/cancers16050981.
[24] D. Liu, X. Che, X. Wang, C. Ma, and G. Wu, “Tumor Vaccines: Unleashing the Power of the Immune System to Fight Cancer,” *Pharmaceuticals*, vol. 16, no. 10, p. 1384, Sep. 2023, doi: 10.3390/ph16101384.
[25] A. Del Prete *et al.*, “Dendritic cell subsets in cancer immunity and tumor antigen sensing,” *Cell. Mol. Immunol.*, vol. 20, no. 5, pp. 432–447, May 2023, doi: 10.1038/s41423-023-00990-6.
[26] A. Decout, J. D. Katz, S. Venkatraman, and A. Ablasser, “The cGAS–STING pathway as a therapeutic target in inflammatory diseases,” *Nat. Rev. Immunol.*, vol. 21, no. 9, pp. 548–569, Sep. 2021, doi: 10.1038/s41577-021-00524-z.
[27] A. R. Hoover *et al.*, “A novel biopolymer synergizes type I IFN and IL-1β production through STING,” Cancer Biology, preprint, Jul. 2022. doi: 10.1101/2022.07.22.501157.
[28] E. S. Pang *et al.*, “Discordance in STING-Induced Activation and Cell Death Between Mouse and Human Dendritic Cell Populations,” *Front. Immunol.*, vol. 13, 2022, Accessed: Mar. 04, 2024. [Online]. Available: https://www.frontiersin.org/journals/immunology/articles/10.3389/fimmu.2022.794776
[29] X. Wang, M. Lin, L. Zhu, and Z. Ye, “GAS-STING: a classical DNA recognition pathways to tumor therapy,” *Front. Immunol.*, vol. 14, 2023, Accessed: Mar. 04, 2024. [Online]. Available: https://www.frontiersin.org/journals/immunology/articles/10.3389/fimmu.2023.1200245
[30] Z. Hu *et al.*, “Glycolysis drives STING signaling to facilitate dendritic cell antitumor function,” *J. Clin. Invest.*, vol. 133, no. 7, Apr. 2023, doi: 10.1172/JCI166031.
[31] J. Wang *et al.*, “STING Licensing of Type I Dendritic Cells Potentiates Antitumor Immunity,” Immunology, preprint, Jan. 2024. doi: 10.1101/2024.01.02.573934.

[32] B. Larkin, V. Ilyukha, M. Sorokin, A. Buzdin, E. Vannier, and A. Poltorak, “Cutting Edge: Activation of STING in T Cells Induces Type I IFN Responses and Cell Death,” *J. Immunol.*, vol. 199, no. 2, pp. 397–402, Jul. 2017, doi: 10.4049/jimmunol.1601999.
[33] R. E. Vatner and E. M. Janssen, “STING, DCs and the link between innate and adaptive tumor immunity,” *Mol. Immunol.*, vol. 110, pp. 13–23, Jun. 2019, doi: 10.1016/j.molimm.2017.12.001.
[34] L. Yu and P. Liu, “Cytosolic DNA sensing by cGAS: regulation, function, and human diseases,” *Signal Transduct. Target. Ther.*, vol. 6, no. 1, p. 170, Apr. 2021, doi: 10.1038/s41392-021-00554-y.
[35] M. Hirschenberger *et al.*, “ARF1 prevents aberrant type I interferon induction by regulating STING activation and recycling,” *Nat. Commun.*, vol. 14, p. 6770, Nov. 2023, doi: 10.1038/s41467-023-42150-4.
[36] Z. Li, S. Cai, Y. Sun, L. Li, S. Ding, and X. Wang, “When STING Meets Viruses: Sensing, Trafficking and Response,” *Front. Immunol.*, vol. 11, p. 2064, Sep. 2020, doi: 10.3389/fimmu.2020.02064.
[37] “Targeting the STING pathway with a combination strategy promotes antitumor activity,” News-Medical. Accessed: Mar. 13, 2024. [Online]. Available: https://www.news-medical.net/news/20230327/Targeting-the-STING-pathway-with-a-combination-strategy-promotes-antitumor-activity.aspx
[38] Q. Liang *et al.*, “Crosstalk between the cGAS DNA sensor and Beclin-1 autophagy protein shapes innate antimicrobial immune responses,” *Cell Host Microbe*, vol. 15, no. 2, pp. 228–238, Feb. 2014, doi: 10.1016/j.chom.2014.01.009.
[39] J. Liu, X. Zhang, and H. Wang, “The cGAS-STING-mediated NLRP3 inflammasome is involved in the neurotoxicity induced by manganese exposure,” *Biomed. Pharmacother.*, vol. 154, p. 113680, Oct. 2022, doi: 10.1016/j.biopha.2022.113680.
[40] M. M. Gaidt *et al.*, “The DNA Inflammasome in Human Myeloid Cells Is Initiated by a STING-Cell Death Program Upstream of NLRP3,” *Cell*, vol. 171, no. 5, pp. 1110-1124.e18, Nov. 2017, doi: 10.1016/j.cell.2017.09.039.
[41] R. Muñoz-Planillo, P. Kuffa, G. Martínez-Colón, B. L. Smith, T. M. Rajendiran, and G. Núñez, “K+ efflux is the Common Trigger of NLRP3 inflammasome Activation by Bacterial Toxins and Particulate Matter,” *Immunity*, vol. 38, no. 6, pp. 1142–1153, Jun. 2013, doi: 10.1016/j.immuni.2013.05.016.
[42] C.-A. Malinczak *et al.*, “Sex-associated early-life viral innate immune response is transcriptionally associated with chromatin remodeling of type-I IFN-inducible genes,” *Mucosal Immunol.*, vol. 16, no. 5, pp. 578–592, Oct. 2023, doi: 10.1016/j.mucimm.2023.06.002.
[43] R. A. Gosavi *et al.*, “Optimization of *Ex Vivo* Murine Bone Marrow Derived Immature Dendritic Cells: A Comparative Analysis of Flask Culture Method and Mouse CD11c Positive Selection Kit Method,” *Bone Marrow Res.*, vol. 2018, pp. 1–9, Feb. 2018, doi: 10.1155/2018/3495086.
[44] L. van de Laar, P. J. Coffer, and A. M. Woltman, “Regulation of dendritic cell development by GM-CSF: molecular control and implications for immune homeostasis and therapy,” *Blood*, vol. 119, no. 15, pp. 3383–3393, Apr. 2012, doi: 10.1182/blood-2011-11-370130.

[45] S. Nair, G. E. Archer, and T. F. Tedder, “ISOLATION AND GENERATION OF HUMAN DENDRITIC CELLS,” *Curr. Protoc. Immunol. Ed. John E Coligan Al*, vol. 0 7, p. Unit7.32, Nov. 2012, doi: 10.1002/0471142735.im0732s99.
[46] PubChem, “HDAC2 - histone deacetylase 2 (human).” Accessed: Mar. 12, 2024. [Online]. Available: https://pubchem.ncbi.nlm.nih.gov/gene/HDAC2/human
[47] A. K. S. Camara, Y. Zhou, P.-C. Wen, E. Tajkhorshid, and W.-M. Kwok, “Mitochondrial VDAC1: A Key Gatekeeper as Potential Therapeutic Target,” *Front. Physiol.*, vol. 8, p. 460, Jun. 2017, doi: 10.3389/fphys.2017.00460.
[48] “LAMP1 - an overview | ScienceDirect Topics.” Accessed: Mar. 14, 2024. [Online]. Available: https://www.sciencedirect.com/topics/biochemistry-genetics-and-molecular-biology/lamp1
[49] “Beta-actin Loading Control | OriGene.” Accessed: Mar. 14, 2024. [Online]. Available: https://www.origene.com/products/antibodies/primary-antibodies/loading-control-antibodies/beta-actin-loading-control
[50] “Histone Deacetylase 2 - an overview | ScienceDirect Topics.” Accessed: Mar. 12, 2024. [Online]. Available: https://www.sciencedirect.com/topics/biochemistry-genetics-and-molecular-biology/histone-deacetylase-2
[51] “STING (D2P2F) Rabbit mAb,” Cell Signaling Technology. Accessed: Mar. 14, 2024. [Online]. Available: https://www.cellsignal.com/products/primary-antibodies/sting-d2p2f-rabbit-mab/13647
[52] B. Hussain *et al.*, “Activation of STING Based on Its Structural Features,” *Front. Immunol.*, vol. 13, p. 808607, Jul. 2022, doi: 10.3389/fimmu.2022.808607.
[53] X. Wu and J. A. Hammer, “ZEISS Airyscan: Optimizing usage for fast, gentle, super-resolution imaging,” *Methods Mol. Biol. Clifton NJ*, vol. 2304, pp. 111–130, 2021, doi: 10.1007/978-1-0716-1402-0_5.
[54] “ZEISS LSM 800 with Airyscan | College of Engineering | University of Nebraska–Lincoln.” Accessed: Mar. 12, 2024. [Online]. Available: https://engineering.unl.edu/nercf/zeiss-lsm-800-airyscan/
[55] J. Huff, “The Airyscan detector from ZEISS: confocal imaging with improved signal-to-noise ratio and super-resolution,” *Nat. Methods*, vol. 12, no. 12, pp. i–ii, Dec. 2015, doi: 10.1038/nmeth.f.388.
[56] “Bit Depth, Full Well, and Dynamic Range - Learn,” Teledyne Photometrics. Accessed: Apr. 03, 2024. [Online]. Available: https://www.photometrics.com/learn/camera-basics/bit-depth
[57] A. M. Bolger, M. Lohse, and B. Usadel, “Trimmomatic: a flexible trimmer for Illumina sequence data,” *Bioinformatics*, vol. 30, no. 15, pp. 2114–2120, Aug. 2014, doi: 10.1093/bioinformatics/btu170.
[58] H. Li *et al.*, “The Sequence Alignment/Map format and SAMtools,” *Bioinformatics*, vol. 25, no. 16, pp. 2078–2079, Aug. 2009, doi: 10.1093/bioinformatics/btp352.
[59] Y. Liao, G. K. Smyth, and W. Shi, “featureCounts: an efficient general purpose program for assigning sequence reads to genomic features,” *Bioinformatics*, vol. 30, no. 7, pp. 923–930, Apr. 2014, doi: 10.1093/bioinformatics/btt656.

[60] G. Yu, L.-G. Wang, Y. Han, and Q.-Y. He, “clusterProfiler: an R Package for Comparing Biological Themes Among Gene Clusters,” *OMICS J. Integr. Biol.*, vol. 16, no. 5, pp. 284–287, May 2012, doi: 10.1089/omi.2011.0118.
[61] “(lysosome death) AND ‘Mus musculus’[porgn] AND (alive[prop]) - Gene - NCBI.” Accessed: Apr. 03, 2024. [Online]. Available: https://www.ncbi.nlm.nih.gov/gene?term=(lysosome+death)+AND+%22Mus+musculus%22%5Bporgn%5D+AND+(alive%5Bprop%5D)&cmd=DetailsSearch&log$=activity
[62] “(NLRP3 inflammasomes pathway) AND ‘Mus musculus’[porgn] AND (alive[pro - Gene - NCBI.” Accessed: Apr. 03, 2024. [Online]. Available: https://www.ncbi.nlm.nih.gov/gene?term=(NLRP3+inflammasomes+pathway)+AND+%22Mus+musculus%22%5Bporgn%5D+AND+(alive%5Bprop%5D)&cmd=DetailsSearch&log$=activity
[63] R. Zhang, R. Kang, and D. Tang, “The STING1 network regulates autophagy and cell death,” *Signal Transduct. Target. Ther.*, vol. 6, no. 1, pp. 1–13, Jun. 2021, doi: 10.1038/s41392-021-00613-4.
[64] D. Bertheloot, E. Latz, and B. S. Franklin, “Necroptosis, pyroptosis and apoptosis: an intricate game of cell death,” *Cell. Mol. Immunol.*, vol. 18, no. 5, pp. 1106–1121, May 2021, doi: 10.1038/s41423-020-00630-3.
[65] Y. Cui *et al.*, “Mycobacterium bovis Induces Endoplasmic Reticulum Stress Mediated-Apoptosis by Activating IRF3 in a Murine Macrophage Cell Line,” *Front. Cell. Infect. Microbiol.*, vol. 6, Dec. 2016, doi: 10.3389/fcimb.2016.00182.
[66] M. M. Gaidt *et al.*, “The DNA Inflammasome in Human Myeloid Cells Is Initiated by a STING-Cell Death Program Upstream of NLRP3,” *Cell*, vol. 171, no. 5, pp. 1110-1124.e18, Nov. 2017, doi: 10.1016/j.cell.2017.09.039.
[67] Z. Yan *et al.*, “The NLRP3 inflammasome: Multiple activation pathways and its role in primary cells during ventricular remodeling,” *J. Cell. Physiol.*, vol. 236, no. 8, pp. 5547–5563, 2021, doi: 10.1002/jcp.30285.
[68] A. Serrano-Puebla and P. Boya, “Lysosomal membrane permeabilization as a cell death mechanism in cancer cells,” *Biochem. Soc. Trans.*, vol. 46, no. 2, pp. 207–215, Apr. 2018, doi: 10.1042/BST20170130.
[69] S. Zhu *et al.*, “Lysosomal quality control of cell fate: a novel therapeutic target for human diseases,” *Cell Death Dis.*, vol. 11, no. 9, p. 817, Sep. 2020, doi: 10.1038/s41419-020-03032-5.
[70] S. Paik, J. K. Kim, P. Silwal, C. Sasakawa, and E.-K. Jo, “An update on the regulatory mechanisms of NLRP3 inflammasome activation,” *Cell. Mol. Immunol.*, vol. 18, no. 5, pp. 1141–1160, May 2021, doi: 10.1038/s41423-021-00670-3.
[71] A. Singhal and S. Kumar, “Neutrophil and remnant clearance in immunity and inflammation,” *Immunology*, vol. 165, no. 1, pp. 22–43, 2022, doi: 10.1111/imm.13423.
[72] Y. Liu *et al.*, “CAPN1 (Calpain1)-Mediated Impairment of Autophagic Flux Contributes to Cerebral Ischemia-Induced Neuronal Damage,” *Stroke*, vol. 52, no. 5, pp. 1809–1821, May 2021, doi: 10.1161/STROKEAHA.120.032749.
[73] “ATP6V0C ATPase H+ transporting V0 subunit c [Homo sapiens (human)] - Gene - NCBI.” Accessed: Mar. 14, 2024. [Online]. Available: https://www.ncbi.nlm.nih.gov/gene/527

[74] "ESCRT-dependent STING degradation inhibits steady-state and cGAMP-induced signalling | Nature Communications." Accessed: Mar. 12, 2024. [Online]. Available: https://www.nature.com/articles/s41467-023-36132-9
[75] X. Cai *et al.*, "Characterization, expression profiling and functional characterization of cathepsin Z (CTSZ) in turbot (*Scophthalmus maximus* L.)," *Fish Shellfish Immunol.*, vol. 84, pp. 599–608, Jan. 2019, doi: 10.1016/j.fsi.2018.10.046.
[76] E.-L. Eskelinen *et al.*, "Role of LAMP-2 in Lysosome Biogenesis and Autophagy," *Mol. Biol. Cell*, vol. 13, no. 9, pp. 3355–3368, Sep. 2002, doi: 10.1091/mbc.E02-02-0114.
[77] Y. Xu, C. Chen, Z. Liao, and P. Xu, "cGAS-STING signaling in cell death: Mechanisms of action and implications in pathologies," *Eur. J. Immunol.*, vol. 53, no. 9, p. 2350386, 2023, doi: 10.1002/eji.202350386.
[78] Z. Xu, Z. Chen, X. Wu, L. Zhang, Y. Cao, and P. Zhou, "Distinct Molecular Mechanisms Underlying Potassium Efflux for NLRP3 Inflammasome Activation," *Front. Immunol.*, vol. 11, Dec. 2020, doi: 10.3389/fimmu.2020.609441.
[79] W. Chi *et al.*, "Caspase-8 promotes NLRP1/NLRP3 inflammasome activation and IL-1β production in acute glaucoma," *Proc. Natl. Acad. Sci.*, vol. 111, no. 30, pp. 11181–11186, Jul. 2014, doi: 10.1073/pnas.1402819111.
[80] L. Liu, Y. Jiang, and J. J. Steinle, "TNFAIP3 may be key to TLR4-activation of the inflammasome in the retinal vasculature," *Exp. Eye Res.*, vol. 220, p. 109108, Jul. 2022, doi: 10.1016/j.exer.2022.109108.
[81] S. Luo *et al.*, "PLCL1 regulates fibroblast-like synoviocytes inflammation via NLRP3 inflammasomes in rheumatoid arthritis," *Adv. Rheumatol. Lond. Engl.*, vol. 62, no. 1, p. 25, Jul. 2022, doi: 10.1186/s42358-022-00252-5.
[82] A. N. R. Weber *et al.*, "Recent insights into the regulatory networks of NLRP3 inflammasome activation," *J. Cell Sci.*, vol. 133, no. 23, p. jcs248344, Dec. 2020, doi: 10.1242/jcs.248344.
[83] N. Samson and A. Ablasser, "The cGAS–STING pathway and cancer," *Nat. Cancer*, vol. 3, no. 12, pp. 1452–1463, Dec. 2022, doi: 10.1038/s43018-022-00468-w.
[84] X. Gui *et al.*, "Autophagy induction via STING trafficking is a primordial function of the cGAS pathway," *Nature*, vol. 567, no. 7747, pp. 262–266, Mar. 2019, doi: 10.1038/s41586-019-1006-9.
[85] H. M. Blevins, Y. Xu, S. Biby, and S. Zhang, "The NLRP3 Inflammasome Pathway: A Review of Mechanisms and Inhibitors for the Treatment of Inflammatory Diseases," *Front. Aging Neurosci.*, vol. 14, Jun. 2022, doi: 10.3389/fnagi.2022.879021.
[86] A. Gritsenko *et al.*, "Priming Is Dispensable for NLRP3 Inflammasome Activation in Human Monocytes In Vitro," *Front. Immunol.*, vol. 11, p. 565924, Sep. 2020, doi: 10.3389/fimmu.2020.565924.

Supplemental Materials

Appendix A: STING-GFP Transfected Cells Materials and Methods

A.1. Materials

DC 2.4 cell line (Millipore Sigma, Cat# SCC142).

A.2. Generation of CRISPR/Cas9 and sgRNA resistant STING1 viral vectors.

First, sgRNA sequences were determined by using Benchling.com. Parameters were set to target the coding sequence with the highest on-target and lowest off-target scores. The following sequences (targeting sequence underlined, mm sgSTING1 #1
sense CACCGCAGTAGTCCAAGTTCGTGCG,
antisense AAACCGCACGAACTTGGACTACTGC; mm sgSTING1 #2
sense CACCGTGAGGGCTACATATTTGGAG,
antisense AAACCTCCAAATATGTAGCCCTCAC; mm sgSTING1 #3
sense CACCGTCCAAGTTCGTGCGAGGCT, antisense AAACAGCCTCGCACGAACTTGGAC) were annealed and ligated into BsmB1 cut LentiCRISPR/eCas9 1.1 Puro.
Briefly, to make a sgRNA resistant mouse STING1 lentiviral expression vector, a Geneblock(IDT) was designed with point mutations in the sgRNA targeting sequence and the PAM sequence for sgSTING1 #1-3. The original amino acid coding sequence was unaltered. PCR amplification of the Geneblock was accomplished using the following primers: Forward 5'-AAGCGCCTCGAGGCCACCATGCCATACTCCAACCTGCATC-3' and Reverse 5'-AAGCGCGAATTCCGTATAAGATGAGGTCAGTGCGGAGTG-3'. PCR amplicon was digested with Xho1 and EcoR1 and ligated into pENTR TagBFP (Evrogen) also digested with Xho1 and EcoR1. The resulting plasmid (pENTR mm sgRes STING1 TagBFP) was then recombined using Clonase II (Thermofisher) into the doxycycline inducible gateway destination lentiviral vector pCW57.1 (Addgene #41393). The resulting lentiviral vector is pCW57.1 mm sgRes STING1 TagBFP. All vector sequences were confirmed using sanger sequencing at the Oklahoma Medical Research Foundation.

A.3. Lentivirus Generation and Transduction

LentiCRISPR/eCas9 1.1 with sgLacZ, sgSTING #1, sgSTING1 #2, sgSTING1 #3 and rescue with sgRNA resistant STING1 overexpression vectors were packaged into lentivirus by co-transfection into HEK 293T cells. Briefly 16ug of DNA [(8ug expression vector, 6ug of PsPax2 (Addgene #12260), and 2ug PMD2.G (Addgene #12259)] was mixed with 64ul of Transporter 5 (Polysciences) in 500ul of OptiMem (Thermofisher). DNA Transporter 5 mix was added to 10cm petri dish of HEK 293T that were nearly confluent. Virus containing medium was collected at 48h and 72h post-transfection and combined. Medium was then filtered using a 0.45micron PVDF syringe filter and concentrated by adding 5% PEG 8000 solution followed by centrifugation at 1500xg for 30 min. Viral containing pellet was resuspended in 500ul of OptiMem. Concentrated viruses were then added to add DC 2.4 in the presence of 10ug/mL of Polybrene. Cells were selected with 10µg/mL of puromycin. Surviving cells were pooled together. Knockout and overexpression was confirmed by Western blotting.

A.4. Results

The knockout was confirmed via western blotting. This can be seen below in **Figure 23**.

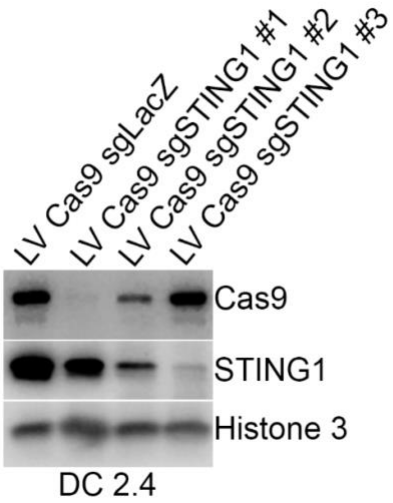

Figure 21: Western blot illustrating STING KO cell lines. LV Cas9 sgLacZ shows expression of STING in a cell line that underwent CRISPR/Cas9 editing without targeting the STING sequencing. LV Cas9 SgSTING1 #1-3 show STING expression in cell lines that underwent CRISPR/Cas9 targeting 3 variations of STING. Histone 3 serves as a control for protein loading, STING 1 shows protein expression, and Cas9 illustrates success of the CRISPR/Cas9 procedures.

A.5. Conclusions

From this several cell lines were created: 1281, 2084, and 2085. The cell line 1281 was a control cell line (CRISPER w/ Lag Z) representing a cell population that had undergone CRISPER genome editing but still contained endogenous STING. The lines 2084 and 2085 are both DC 2.4 cell lines with different levels of STING expression. Cell line 2084 corresponds with LV Cas9 sgSTING 1 #2 in **Figure 23** and correlates with an 80% deletion of endogenous STING. Cell line 2085 corresponds with LV Cas9 sgSTING 1 #3 in **Figure 23** and correlates with approximately a 95% deletion of endogenous STING.

While both STING-GFP and STING-KO cell lines were created, the STING-KO cell lines (1281, 2084, and 2085) were utilized in the initial testing. This initial testing consisted of IL-1β and IFN-β enzyme-linked immunosorbent assays (ELISA). The methodology, results, and conclusions of these procedures can be seen in **Appendix B.**

Appendix B: STING KO Procedures and Results

B.1. Materials

DC 2.4 cell line (Millipore Sigma, Cat# SCC142). STING-KO DC 2.4 lines 1281, 2084, and 2085 (protocols for cell line derivation can be found above in **Appendix A**).

B.2. Methods

A 96 well plate was utilized throughout the procedure. Plate preparation is as follows: GC stimulation concentrations were made, 10µl of GC solution and 200µl of cells at a 1million/mL cell suspension were added to the appropriate wells, and the plate was allowed to incubate overnight at 37°C. Post incubation supernatants were collects for use within ELISA protocols. Below **Table 4** illustrates how GC concentrations were made. The stock solution was dilution by 1/100 and 1/10 to make the 0.8µg/mL and 4-32µg/mL concentrations respectively.

Table 4: GC Concentration Preparation

Concentration	0.8	4	8	16	32	64
GC Stock (µl)						25.6
1/10 (µl)		16	32	64	128	
1/100 (µl)	32					
Media (µl)	168	184	168	136	72	174.4

The ELISAs were conducted using kits purchased from R&D Systems and Thermo Fisher. ELISAs run include IL-1β (Thermo Fisher, Cat#88-7013-22) and IFN-β (R&D systems, Cat#MIFNB0). Kits were conducted as per manufacture protocols. Analysis was conducted using GraphPad Prism.

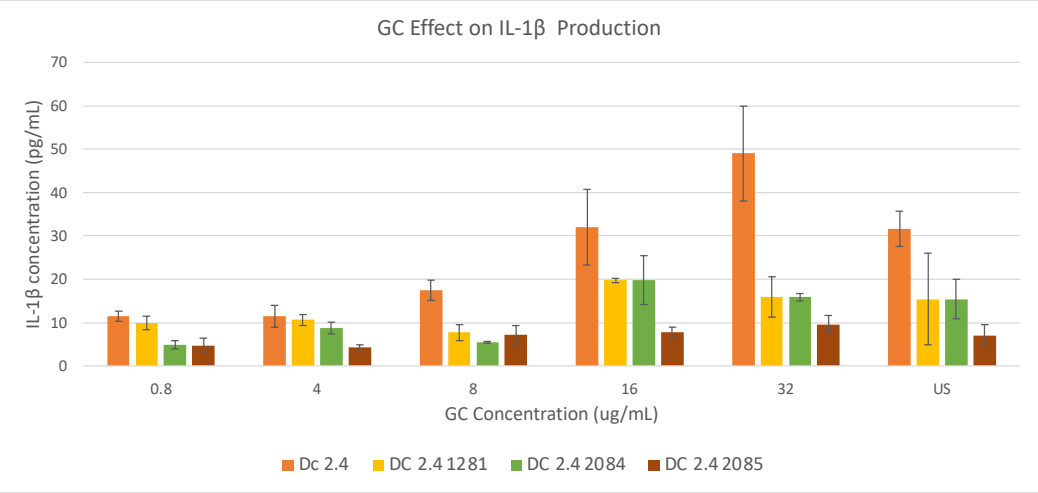

Figure 22: First iteration of IL-1β ELISA. Four different cell lines were utilized, two STING KO lines and two control lines. Six different GC concentrations were tested. The general trend here aligns with prior data collected in our lab.

B.3. Results: ELISA on STING KO

Several iterations of IL-1β and IFN- β ELISAs were conducted. The results from these trials can be seen below. The first iteration yielded the expected trend if cytokine production. However, in subsequent trials, this trend was no longer observed.

The first iteration of the IL-1β ELISA yielded the expected trend aligning with cytokine production from our prior experimentation. However, following iterations did not show any significant cytokine production, with absorbances reading close to 0. The absorbance results from these trials can be seen below in **Tables 5-7**.

Table 5: ELISA IL-1β #2

	DC 2.4				1281				2084				2085			
US	0.141	0.051	0.059	0.075	0.051	0.048	0.049	0.044	0.139	0.04	0.124	0.05	0.045	0.06	0.097	0.038
0.8	0.043	0.036	0.04	0.038	0.038	0.041	0.033	0.033	0.033	0.036	0.035	0.035	0.033	0.045	0.031	0.043
4	0.02	0.032	0.029	0.03	0.033	0.03	0.041	0.037	0.028	0.029	0.047	0.029	0.031	0.053	0.033	0.036
8	0.037	0.03	0.031	0.027	0.029	0.03	0.03	0.03	0.03	0.031	0.028	0.03	0.032	0.031	0.033	0.035
16	0.039	0.038	0.033	0.038	0.031	0.032	0.033	0.033	0.031	0.029	0.03	0.029	0.031	0.034	0.032	0.478
32	0.034	0.035	0.036	0.03	0.031	0.033	0.031	0.029	0.031	0.03	0.03	0.046	0.029	0.033	0.303	0.042
64	0.038	0.036	0.03	0.03	0.033	0.039	0.03	0.035	0.031	0.045	0.031	0.041	0.034	0.032	0.035	0.049

Table 6: ELISA IL-1β #3

	DC2.4				1281				2084				2085			
US	0.016	0.016	0.017	0.017	0.017	0.018	0.016	0.018	0.017	0.017	0.019	0.017	0.019	0.018	0.018	0.018
0.8	0.019	0.019	0.019	0.017	0.018	0.017	0.017	0.018	0.017	0.017	0.017	0.019	0.017	0.017	0.016	0.019
4	0.018	0.02	0.02	0.019	0.018	0.018	0.023	0.019	0.02	0.018	0.018	0.018	0.019	0.019	0.018	0.018
8	0.018	0.017	0.021	0.021	0.021	0.02	0.021	0.025	0.019	0.026	0.019	0.025	0.019	0.034	0.021	0.021
16	0.017	0.018	0.02	0.021	0.021	0.02	0.022	0.022	0.023	0.022	0.022	0.022	0.02	0.02	0.018	0.019
32	0.015	0.019	0.02	0.02	0.021	0.018	0.02	0.019	0.02	0.018	0.02	0.019	0.021	0.02	0.02	0.02
64	0.017	0.018	0.02	0.02	0.018	0.02	0.019	0.019	0.018	0.019	0.019	0.018	0.019	0.02	0.019	0.02

Table 7: ELISA IL-1β #4

	DC 2.4		1281		2084		2085	
US	0.018	0.019	0.019	0.018	0.02	0.022	0.021	0.018
0.8	0.018	0.019	0.019	0.018	0.02	0.02	0.019	0.02
4	0.018	0.017	0.018	0.018	0.018	0.019	0.02	0.018
8	0.019	0.018	0.018	0.018	0.018	0.019	0.018	0.02
16	0.022	0.021	0.019	0.018	0.02	0.021	0.019	0.018
32	0.018	0.019	0.019	0.019	0.019	0.02	0.019	0.02
64	0.02	0.02	0.02	0.019	0.019	0.02	0.019	0.018

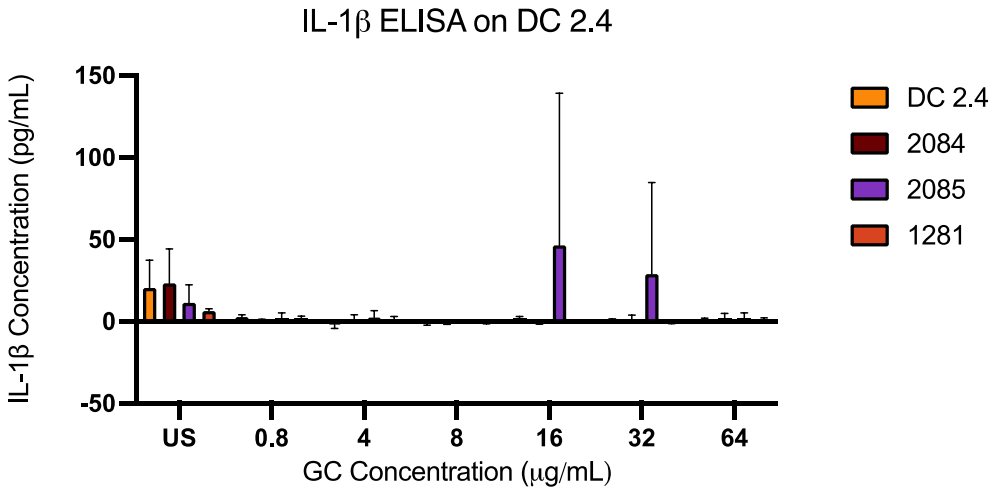

Figure 23: IL-1β ELISA on STING KO STING lines. No detectable trend can be seen and most of data falls below the detectable range of protein concentrations. DC 2.4 and 1281 are the control cell lines while 2085 is a 80% KO and 2085 is a 90% KO.

The absorbances from the ELISA trials can be seen above in **Tables 5-7**. These absorbances primarily registered below the standard curves placing them out of range for protein detection. Below, **Figure 25** shows the measured concentration from one such trial.

Inconsistencies in the IL-1β results prompted the investigation of another cytokine. IFN-β was chosen as the lab we have seen consistent expression of this proinflammatory cytokine by DC 2.4 before. However, the absorbances for these trials were also below the detectable protein range. The results from these trials can be seen below in **Tables 8-9.**

Table 8:ELISA IFN-β #1

	DC 2.4		1281		2084		2085	
US	0.019	0.022	0.019	0.018	0.031	0.026	0.018	0.018
0.8	0.018	0.018	0.029	0.031	0.103	0.111	0.018	0.018
4	0.017	0.017	0.059	0.062	0.425	0.495	0.016	0.017
8	0.017	0.017	0.033	0.027	0.584	0.791	0.019	0.019
16	0.02	0.019	0.029	0.024	0.484	0.685	0.021	0.024
32	0.02	0.039	0.026	0.028	0.483	0.529	0.022	0.026
64	0.019	0.102	0.032	0.024	0.169	0.276	0.019	0.021

Table 9: ELISA IFN-β #2

	DC 2.4		1281		2084		2085	
US	0.021	0.02	0.021	0.021	0.021	0.017	0.018	0.019
0.8	0.022	0.023	0.029	0.034	0.02	0.022	0.021	0.025
4	0.022	0.022	0.067	0.075	0.081	0.115	0.03	0.027
8	0.024	0.021	0.053	0.045	0.566	0.347	0.053	0.058
16	0.023	0.021	0.043	0.041	1.324	1.534	0.076	0.079
32	0.024	0.021	0.036	0.036	1.855	1.812	0.075	0.094
64	0.023	0.022	0.029	0.027	0.407	0.247	0.029	0.03

B.4. Discussion and Conclusions

While the first IL-1β yielded the predicted trend, the results were unable to be replicated. Following this iteration, all other ELISAs showed no detectable cytokine concentrations. While the subsequent iterations showed no cytokine presence, the controls and standard curves present as expected indicating the ELISA itself was functioning as expected.

From the ELISA data two main conclusions can be drawn. First, the control cell line for the STING KO cell line did not behave consistently with the DC 2.4 cell line. This showed that the act of Cas9 gene editing changed the native behavior of the cells. Secondly, the DC 2.4 cell line did not behave as expected. In prior experiments, we have seen a consistent expression of IL-1β and IFN-β by DC 2.4 when stimulation with concentration at of higher then 8μg/mL. As this trend was no longer being observed, it was hypothesized that there may be inconsistencies within the cell line. This prompted the use of BMDCs for the remainder of the experimentation. As this cell line would more closely mimic the native murine environment.

Appendix C: Optimization of Lysate Protocols

The beforementioned subcellular fractionation and lysosomal isolation are conducted utilizing kits design for human cells. As these kits were being applied to murine cells optimization was required to ensure kit efficacy was maintained. Optimization studies were conducted on the DC 2.4 cell line (Millipore Sigma, Cat# SCC142) and once protein levels optimal for western blotting was achieved, the protocols were applied to murine primary cells.

The cellular fractionation kit called for a cell count of 1-10 x 10^6 cells to be utilized throughout the protocol. While 10 x 10^6 yielded detectable lysates, with acceptable protein concentrations demonstrated by the BCA, the volume was insufficient to create western blot lysates. Iterative trials showed that the lysate volume yielded from greater than 20 x 10^6 cells would suffice. Increased cell count utilized within the protocol increased volumetric output of lysate while maintaining protein potency. This trend is demonstrated below in **Figure 8**.

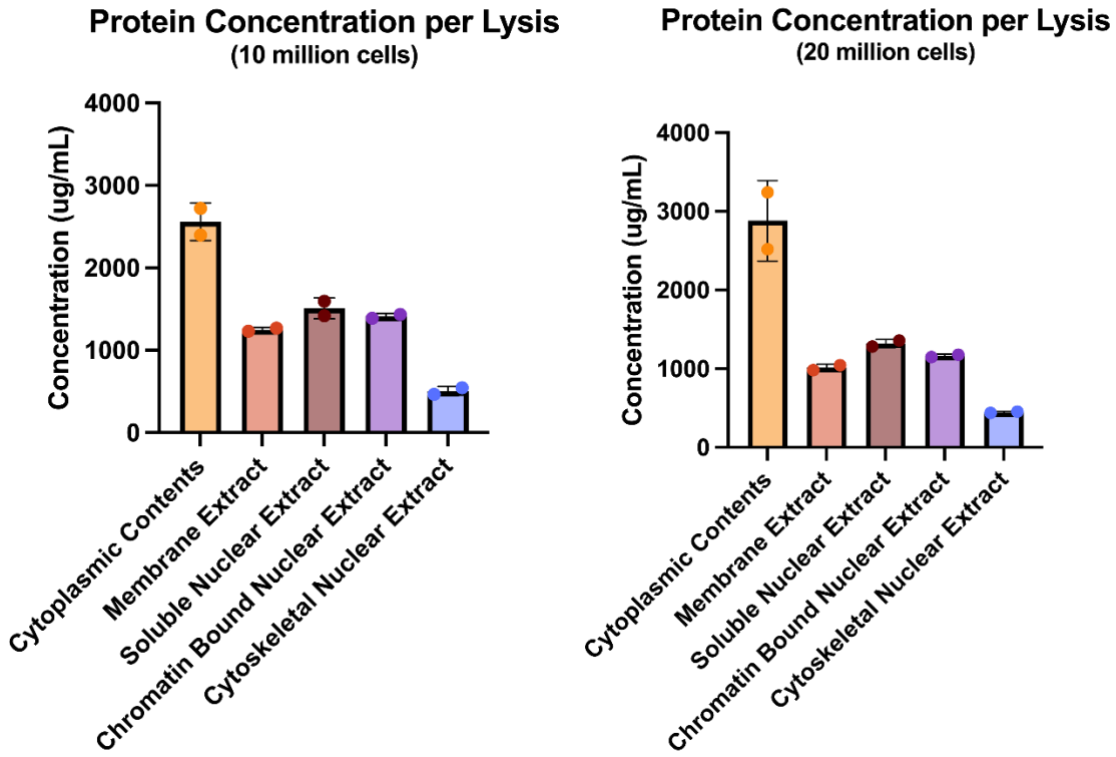

Figure 24: Cellular Fractionation BCA. BCA results from cellular fractionation on DC 2.4 cell line utilizing 10 million and 20 million cells. Higher cell count yielded a larger volume of lysate but maintained protein potency ideal for western blotting applications.

The lysosomal isolation called for 50-200mg of cells to be utilized for the procedure. Initially 50 x10^6 cells were used for the procedure. However, this did not yield a lysosomal pellet. In the subsequent iterations approximately 150 x10^6 cells were used yielding 80-110mg cell pellets. These cell concentrations yielded a visible cell pellet but protein concentrations were too low to be used for western blot procedures. A cell pellet with optimal protein concentration was yielded with approximately 200 x10^6, this was used as the target cell count for all subsequent iterations of the protocol.

Appendix D: Cellular Magnification Microscopy Methodology

D.1. Materials

A GC-FITC aqueous solution (10mg/mL) was provided by ImmunoPhotonics. DC 2.4 cell line (Millipore Sigma, Cat# SCC142).

D.2. Methods

Coverslips (18mm, #1 glass) are treated using piranha solution (3:1 ratio of 95-98% sulfuric acid and 30% hydrogen peroxide). Coverslips were then placed into individual wells of a 12 well plate and wells washed with PBS. The plate was then treated with UV light for 10 minutes and stored at 4°C for later use. Upon use, the plate was treated again with UV light for 10 minutes.

Cells were seeded at a density of 500,000 cells per well and stimulated with GC. Three experimental groups were tested: unstimulated, 4μg/mL GC-FITC, and 8μg/mL GC-FITC. Samples were incubated with GC for a total stimulation time of 10 hours. Post stimulation, cells were fixed with 4% PFA and 0.1% glutaraldehyde in 1X PBS for 15 min at room temperature. Samples were then rinsed 3 times with PBS. Post fixing, samples were quenched to help reduce background signal. For quenching 1 mg/mL solution of sodium borohydride in PBS was added for 10 minutes at room temperature. Next, 100 mM glycine in PBS was added for 20 minutes at room temperature followed by an additional rinsing of PBS. Lastly, samples were rinsed 3 times with PBS.

Following quenching, the samples went through gelation. During this process, an acrylamide gel was added to the samples. In doing this, the cells were incorporated into the gels allowed for expansion of the samples. The gelling solution was prepared as follows: 0.416 mL of N,N-Dimethylacrylamide (DMAA), 3.4 g of sodium acrylate, 1 g of acrylamide (2.5 mL of 40% solution), 50 µl of bisacrylamide (2% solution): 1 mg, 0.1 g sodium chloride, 1 mL of 10X PBS, and water up to 10 mL. For every 1mL of gelling solution, 50µL 5% potassium persulfate (KPS), 10µL 10% TEMED solution, and 1µL methacrolein is added. For each sample 90µL of gelation solution was added and allowed to gelate in the humidified gelation chambers overnight at 37°C.

The homogenization solution was prepared as follows: 5 g sodium dodecyl sulfate (SDS), 24.024 g of urea, 365.3 mg EDTA, 10 mL of 10X PBS, Nanopure up to 50mL. The pH was the adjusted to 7.5. The homogenization buffer was then added to each well and incubated for 6 hrs at 80°C. Post incubation, samples were washed with PBS 3 times for 10 minutes each at room temperature.

Post homogenization, samples were stained with primary antibodies: STING 1° Rabbit mAb (1:100) (Cell Signaling, Cat#13647S) and LAMP 1° (1:100) (Thermo Fisher, Cat#14107182). Samples were allowed to incubate at room temperature on the shaker overnight. Following incubation samples were washed 3 times with 0.1% PBS-T for 20 minutes each wash then sained with secondary antibodies. For secondary antibodies the following were used: Cyanine5 (1:1000) (Thermo Fisher, Cat#A10525) and Alexaflour 555 (1:500) (Thermo Fisher, Cat#A32732). Antibodies were allowed to incubate overnight on the shaker at room temperature. Post incubation samples were washed 3 times for 20 minute durations with 0.1% PBS-T before pan staining. Pan staining was conducted utilizing a solution compromised on 20μg/mL N-

Hydroxysuccinimide (NHS) ester-activated fluorescent dye (NHS-AF555) and 100mM of sodium bicarbonate. The solution was applied to the samples, allowed to incubate at room temperature with shaking for 1.5 hours, and then washed 3 times for 20 minute durations with 0.1% PBS-T. A final wash for 1 hour was conducted with 1X PBS.

Following staining samples were expanded. For expansion, gels were placed in Nanopure H_2O for 10 minutes thrice, replacing the water each time, or until expansion stops. Samples were then imaged on the Oxford Instruments Andor BC43 Confocal Microscope.

D.3. Results

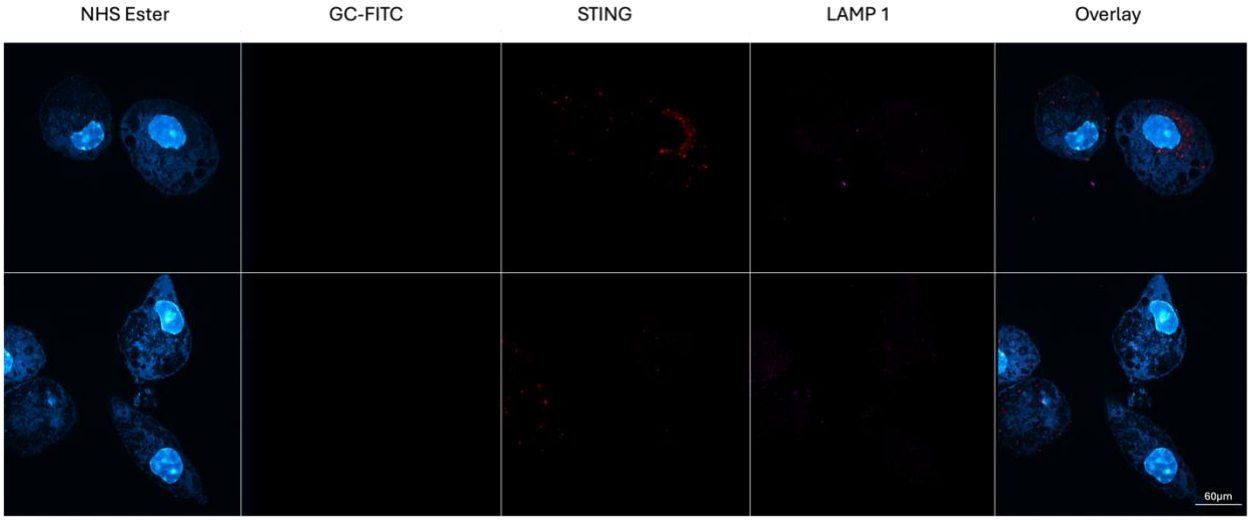

Figure 25: Unstimulated DC 2.4 Expansion Microscopy. Shows antibody staining with STING-AF55 and LAMP1-Cy5. GC-FITC showing GC presence in the cell and NHS ester staining proteins within the cell can also be seen.

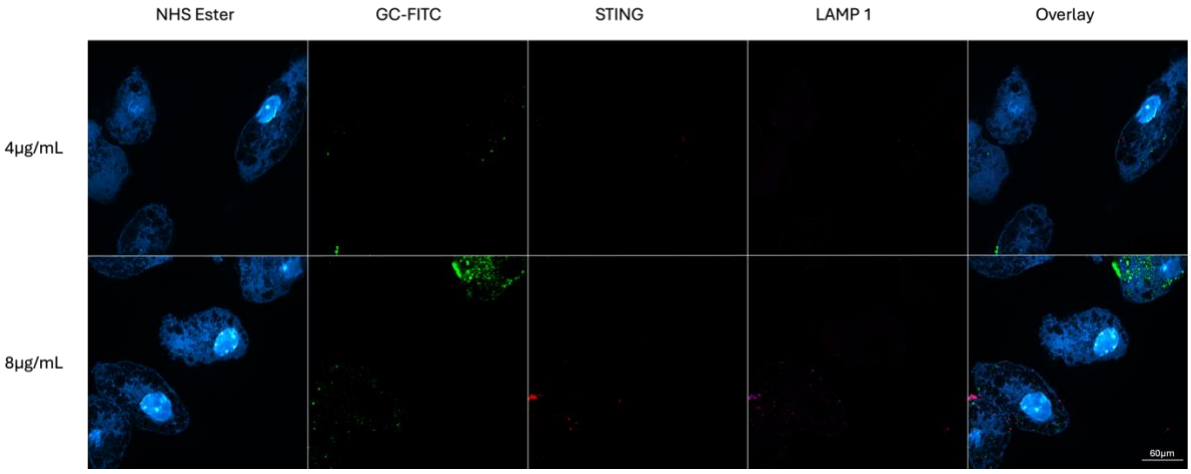

Figure 26: 4µg/mL and 8µg/mL DC 2.4 Expansion Microscopy. Shows antibody staining with STING-AF55 and LAMP1-Cy5. GC-FITC showing GC presence in the cell and NHS ester staining proteins within the cell can also be seen. Two different stimulation concentrations of GC can be seen here.

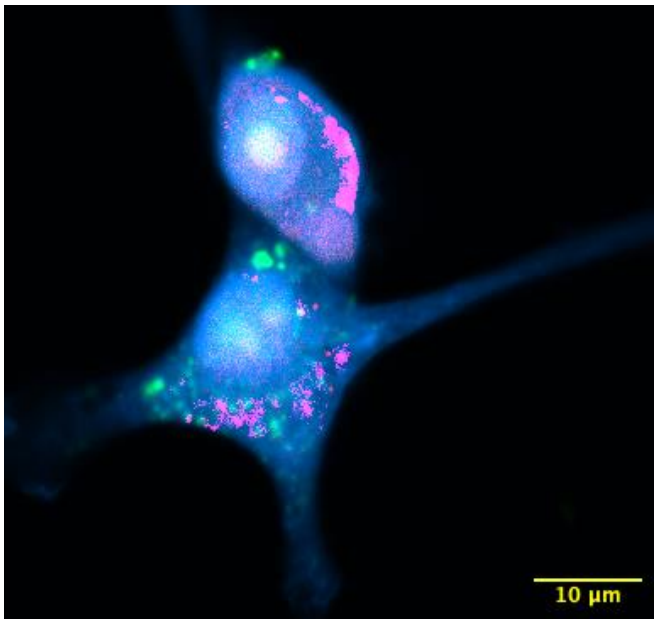

Figure 27: 4µg/mL non-expanded DC 2.4 microscopy. Shows overlay of nonexpanded sample. STING and LAMP1 expression can be seen (red and magenta respectively). GC-FITC (green) shows GC presence in the cell at a concentration of 4µg/mL. NHS marks the proteins in the cell and can be seen by the blue expression in the image.

D.4. Discussion and Conclusions

The expansion of the DC 2.4 line was successful and GC-FITC was well preserved during the expansion. This resulted in better visualization of the subcellular components within the DC 2.4s and held promise for investigating GC and STING colocalization within the lysosome. However, it can be seen by comparison of **Figure 26-28** there are limitations with the antibody staining. In **Figure 28** clear antibody tagging with STING and LAMP 1 can be seen while in **Figure 26** and **Figure 27** the expression in greatly decreased. This is likely due to the gel being difficult to penetrate. Antibody staining occurs after the gelation steps meaning the stains need to fully penetrate through the gel. This physical barrier can limit the success of the tagging. Combined with the large amount of antibody this procedure required, an alterative method of imaging was investigated. Airyscan imaging was chosen for subsequent procedures as it allowed for an increase of resolution, allowing for the visualization of subcellular components without the need for expansion.

Appendix E: Macro for Particle Analysis

The code utilized for particle analysis can be seen below. This outlines the steps taken in ImageJ to threshold and count the particles for both the GC-FITC and STIN-AF555 channels. The results were exported to excel and analyzed for particle overlap.

```
open("/Users/ghainaa/Desktop/Particle Analysis /Particle Analysis 4ugmL s2 2/4ug mL processed s2 2.czi");
selectWindow("4ug mL processed s2 2.czi - C=2");
setOption("ScaleConversions", true);
run("8-bit");
run("Duplicate...", " ");
//set FITC channel to 8-bit and duplicate
selectWindow("4ug mL processed s2 2.czi - C=1");
setOption("ScaleConversions", true);
run("8-bit");
run("Duplicate...", " ");
//set STING channel to 8-bit and duplicate
selectWindow("4ug mL processed s2 2.czi - C=1-1");
//run("Threshold...");
setAutoThreshold("Otsu dark no-reset");
//setThreshold(40, 255);
setOption("BlackBackground", true);
run("Convert to Mask");
//applies threshold of "Ostu" and B&W" to duplicate of STING channel
selectWindow("4ug mL processed s2 2.czi - C=2-1");
setAutoThreshold("Otsu dark no-reset");
//run("Threshold...");
//setThreshold(46, 255);
run("Convert to Mask");
//applies threshold of "Ostu" and B&W" to duplicate of FITC channel
run("Set Scale...", "distance=23.5285 known=1 unit=pixel global");
//changes sclaing to pixels
run("Set Measurements...", "area mean redirect=[4ug mL processed s2 2.czi - C=2] decimal=3");
//sets measurments to give mean grey value redirected on the FITC channel (gives value in terms of fluorescence  detected on FITC channel)
run("Analyze Particles...");
run("Analyze Particles...", "  show=Outlines display overlay add composite");
//runs particle analysis from particle size 0-Infinity on FITC particles projected onto FITC channel to gather information for thresholding
run("Analyze Particles...", "size=6-750 show=Outlines display overlay add composite");
//runs particle analysis from particle size 6-750 on STING particles projected onto FITC channel for overlap analysis

```

Figure 28: Code delineating the procedure for GC-FITC and STING overlap. The steps of converting the images to 8 bit, thresholding each image, and running particle analysis can be seen.

Appendix F: Cell Size Analysis

F.1. Methods

While swollen vesicles were an observed result of GC stimulation, it was unclear if this results in an overall cell volume changed. In order to test this, cell size analysis was run. Freehand drawing was chosen as the method of analysis as the analysis required specific cell selection. The cells that phagocytosed GC were the cells that underwent swollen vesicle formation. These were the cells that required cell size analysis. Due to the specific nature of the analysis, freehand provided the most accurate analysis.

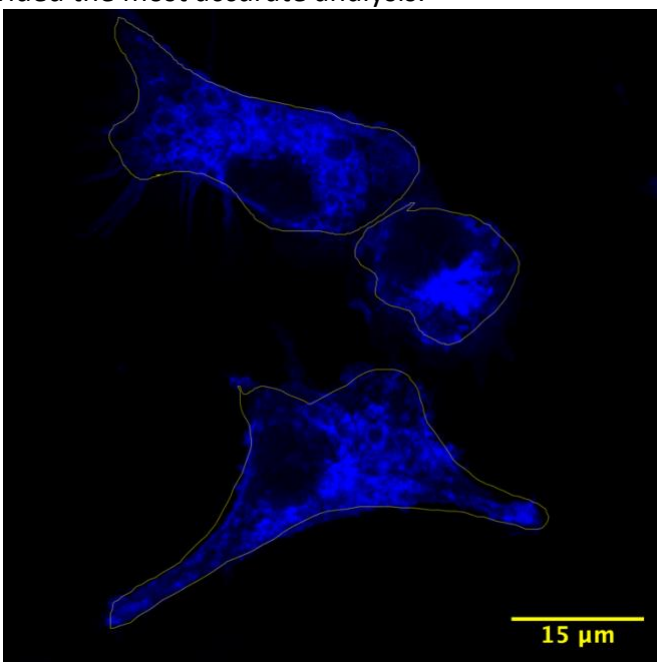

Figure 29: Cell Size Analysis on Unstimulated BMDC. Shows freehand cell size analysis on cells within the field of view. Cells were outlined in this manner then cell area was derived using ImageJ.

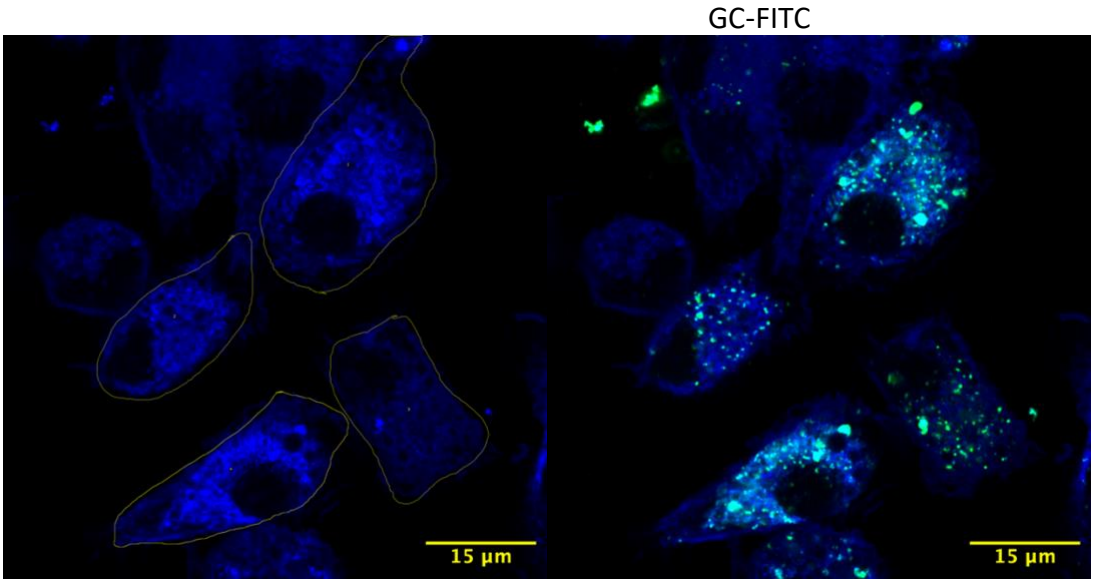

Figure 30: Cell Selection for Analysis. Cell that phagocytosed GC were chosen for analysis. This can be seen where 4 cells in the GC-FITC channel show GC uptake. These cells were chosen for analysis via freehand ROI.

F.2. Results

After freehand ROI of cells of interest were taken, the ROI area was taken. For each sample analyzed 2-4 cells were in the field of view and available for analysis. The cell areas can be seen below in **Table 10**.

Table 10: Cell Size Analysis

	US			4µg/mL			8µg/mL		
Cell Area 1	411.286	327.594	829.88	502.21	533.444	677.374	262.016	337.009	504.461
Cell Area 2	193.274	506.686	648.304	269.645	267.867	277.206	449.561	134.207	251.106
Cell Area 3	437.554	227.605		314.859		243.207		379.527	246.568
Cell Area 4				344.083				342.269	
Average	**347.371333**	**353.961667**	**739.092**	**357.69925**	**400.6555**	**399.262333**	**355.7885**	**298.253**	**334.045**

F.3. Discussion and Conclusions

No significant difference in cell size were detected as seen in **Table 10**. This could be due to several factors more time points and concentrations of GC would be required to gain further insight.

Appendix G: ROI Particle Analysis

G.1. Methods

The whole field of view encompasses several different stages of the cellular processes as not all the cells will be on the same timescale. Each cell will uptake GC at a slightly different timepoint. Due to this, single cell overlap analysis was also conducted. ROIs within the field of view were taken and then analyzed for overlap. The ROI selection process was as follows. Cells with large amount of cellular swelling were not selected as the swelling was indicative of cellular stress. Vesicle swelling would be downstream of GC-STING interactions, therefore cells indicating GC-STING interactions without cellular swelling were chosen for analysis. ROIs were selected from both the 4μg/mL and the 8μg/mL experimental groups. An example of a suitable ROI chosen for particle analysis is shown below in **Figure 29.**

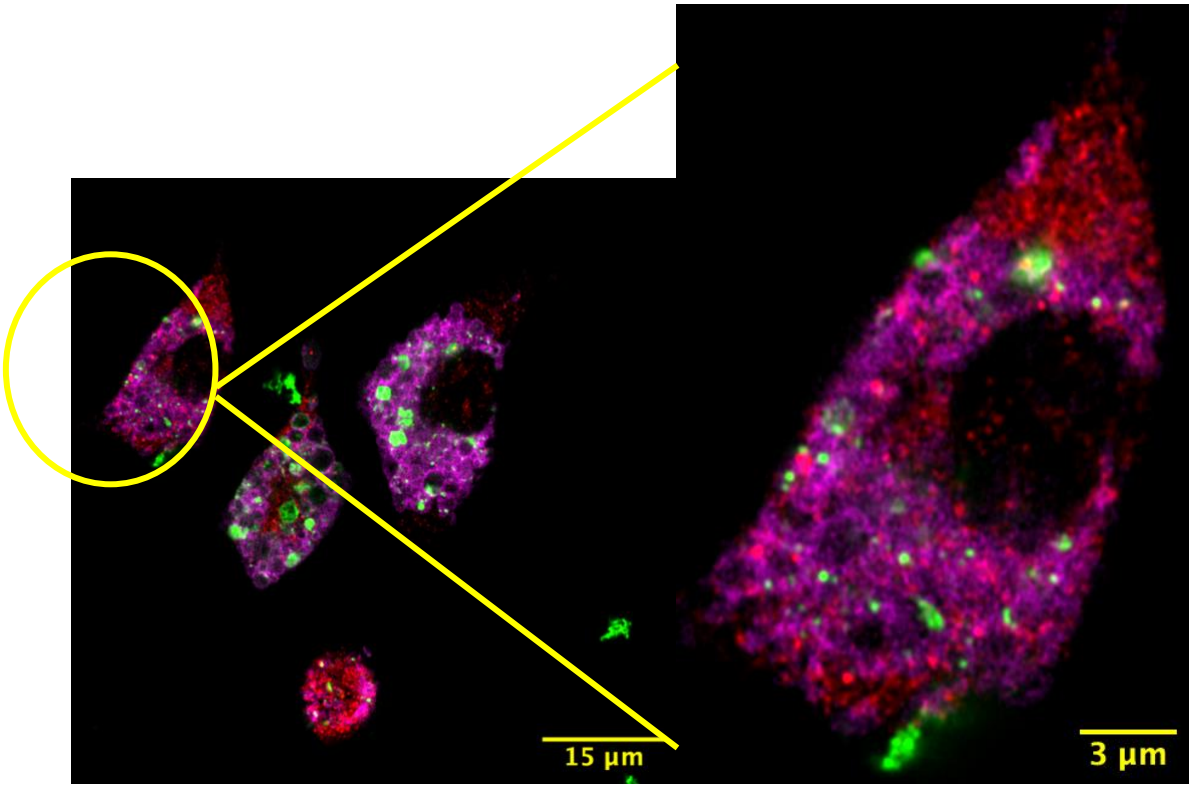

Figure 31: **Shows ROI selection criteria**. Image depicts overlap of BMDC stimulated with 8μg/mL GC-FITC. STING (red), LAMP 1 (magenta), and GC-FITC (green) are overlapped within the image. The selected ROI shows a cell that has good uptake of GC but has not yet undergone cellular swelling.

Utilizing the ROI selection process above, particle analysis was re-run to gather GC-FITC overlap data. The methodology for this analysis can be seen in above in **Chapter 4.**

G.2. Results and Conclusions

Overlap analysis on ROI were similar to that of the whole cell analysis seen in **Chapter 4**. Different concentrations and time points would be required to gain further insight.